UNIVERSITY OF COPENHAGEN
DEPARTMENT OF GEOSCIENCE AND NATURAL RESOURCE MANAGEMENTS

Field and Methods course, Disko, 2024

Foreword

Every second year, the Department of Geoscience and Natural Resource Management at the Faculty of Science of the University of Copenhagen arrange a *Field and Method Course* in arctic physical geography at Arctic Station, Qeqertarsuaq on Disko Island. In 2024, a group of 14 students participated in the field course at the end of August.

The course included a presentation of relevant methods, a hands-on use of methods, and a research project in the field. Here, the students worked in groups and took lead in data collection, data preparation and discussion of the results. The projects have been carefully prepared for months in advance.

The themes of *Field and Method Course 2024* included: marine and lake coring, mercury deposition and sedimentation rates, landscape geomorphology, production and consumption and net exchange of greenhouse gases from a proglacial landscape near the retreating Lyngmarksbræen as well as from a landscape gradient in Blæsedalen. Measurements included both methane and nitrous oxide in the field and as part of laboratory incubations.

All students have completed the course and this report includes the findings of the projects written as four scientific papers.

Many thanks to 14 enthusiastic students, the staff at Arctic Station and Arctic Station board secretary Gitte Henriksen. Parts of the course were directly linked to MOMENT and Centre for Permafrost and included not the least excellent support and supervision by professor Lars Kutzbach and Dr. Claudia Fiencke from University of Hamburg and Dr. Peiyan Wang from Department of Geoscience and Natural Resource Management at University of Copenhagen. Additional data has been made available by Charlotte Sigsgaard through the Arctic Station monitoring program and Greenland Ecosystem Monitoring (GEM).

November 2024,

Thorbjørn Joest Andersen and Bo Elberling

Tabel of content

Mercury pollution in Disko Bay

Louise Rye Svendsen, Simone Schroll Jønsson, Victoria Bjerre Hansen & Zhichao Xiong

Abstract

There has been a global increase in the emission of mercury since the industrial revolution, as mercury gets deposited in the arctic leading to bioaccumulation. Through an investigation of a sediment core from Egedesminde dyb in Disko bay, Greenland, dated with ^{210}Pb, this paper aims to investigate if climate change has had an effect on the pollution of mercury in the arctic. This paper shows that there are no direct links between the increasing pollution and mercury in the arctic and the rising temperature. Instead, the measured increase in mercury from 1874-2014 correlate to the increase in anthropogenic mercury emission. The sediment size and organic content of the sediment core were also investigated.

Introduction

Climate change refers to long-term changes in temperature and weather patterns, caused mainly by human activities such as the burning of fossil fuels, deforestation, and industrial processes. The impacts include increases in global temperatures, melting ice caps, increases in extreme weather events, and disruption of ecosystems. Since 1958, global temperatures have seen a significant increase and by the end of the 20th century, the average global temperature had risen by approximately 0.8°C (Lindsey and Dahlman, 2024). During recent decades, Arctic warming has been two to three times larger than the global mean near surface air temperature trend (Masson-Delmotte et al., 2012).

In addition to the increase in temperature, the emissions of heavy metals (Hg, Cd, Pb, et.) into the atmosphere have increased since the onset of industrialisation (AMAP, 2011; McConnell and Edwards, 2008). The main causes are human activities e.g. burning of fossil fuels and natural causes such as volcanic eruptions (Mason and Sheu, 2002; Selin et al., 2007). These metals can bioaccumulate in living organisms, which increases the concentrations and toxic effects in higher trophic levels (Chouvelon et al., 2019; Harding et al., 2018).

Mercury from sediment cores has been studied previously (Bindler et al., 2001; Asmund & Nielsen, 2000) and it is clear that the main causes of the high mercury content in the Arctic originates from anthropogenic emissions. However, as the climate changes and temperature increases in the Arctic (Masson-Delmotte et al., 2012), it is interesting to investigate if the changing climate could be an additional contributor to the mercury pollution. This study aims to analyse the evolution of mercury pollution in relation to climate change in Greenland through a case study at Egedesminde Dyb in Disko Bay.

Theory

Climate and climate change in Greenland

Greenland is located within the Arctic Circle. Greenland's climate displays distinct regional and seasonal patterns, as

temperature and precipitation are higher in the south than in the north and lower in summer compared to winter. Additionally, significant climatic variations exist between the outer coast and the inner fjords. The mean annual temperature at the southern part of Greenland's coast is ~1.3 °C (Westergaard-Nielsen et al, 2019). In summer, the maximum precipitation reaches up to 600 mm/year. In winter, the maximum snowfall peaks at up to 1500 mm/year (Fettweis et al., 2017).

The climate in Greenland has generally had a warm climate trend during the last two decades. The sea surface temperatures in the Southwest have risen by ~0.5°C in winter and ~1°C in summer (Masson-Delmotte, 2012). This has led to significant melting of Greenland's glaciers, which directly contributed to the global sea level rise (Yaqiong Mu et al., 2020).

Mercury

Mercury is toxic even at very low concentrations and even more so in its methylated form MeHg (Jackson, 1998). Furthermore, the methylated form of mercury has a higher bioavailability, which in aquatic environments leads to an increased accumulation of mercury in the food network (Jackson, 1998).

Previous research in the Arctic has utilised sediment cores in order to measure the level of Hg through time (Bindler et al., 2001; Asmund & Nielsen, 2000). Here Bindler et al. (2001) found that the pre-industrial revolution (about 1700) was the first major increase in measured Hg. Furthermore, the amount of Hg was found to have had its maximum accumulation rate in the 1970's and 1980's, and the lakes closest to the Greenland Ice Sheet have the highest concentration compared with those further away (Binder et al., 2001). Asmond and Nielsen (2000) found that the mercury levels had doubled in marine sediments from 1900 to 2000 indicating that the mercury was of anthropogenic origin (Asmund & Nielsen, 2000). The emissions of Hg to the environment in the period 1510-2010 are illustrated in Figure 1.

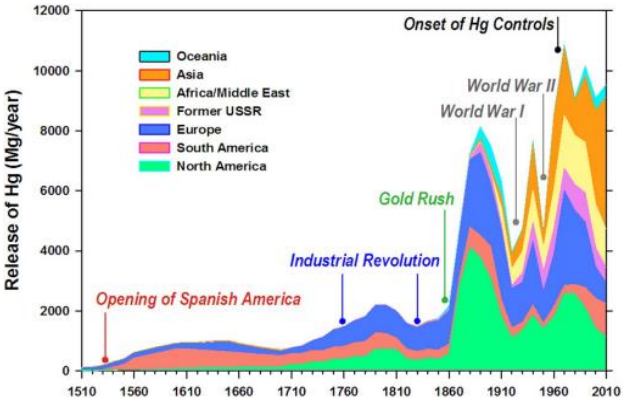

Figure 1: The release of Hg to the environment in the period 1510-2010. Source: Streets et al (2019).

Transport of Mercury to the Arctic

Most mercury in the Arctic originates from other regions in the world. This is largely due to mercury's gaseous form Hg(0) remaining within the atmosphere for 6 months to 1 year (Horowitz et al., 2017). Mercury introduced to the arctic environment is emitted within the northern hemisphere and transported in the atmosphere, or by marine currents and river outflows (AMAP, 2021). The movement of Hg through ocean currents occurs in the time span of years to decades from the mid-latitudes (Tovgaard et al., 2024).

Mercury sources and sinks

In 2018 the Global Mercury Assessment (UN Environment, 2019) covered the current sources of mercury emissions. It was here found that approximately 30 % of

the emissions are anthropogenic in origin, 10 % are from natural sources, and the remaining 60 % is re-released mercury. There is no distinction between re-released mercury from landfills and plants. The current high rate of re-released mercury is, however, partly due to previous high rates of anthropogenic emission (AMAP, 2021).

There are two types of deposition of Hg from the atmosphere, dry and wet deposition. Dry deposition is mainly from the gaseous form of mercury Hg(0), that is absorbed by plants via stomatal and cuticular pathways and later deposited in the soil by roots and fallen leaves (AMAP, 2021). Dry deposition has been measured to both be deposited over terrestrial and oceanic areas and is responsible for 71 % of deposition within the arctic (AMAP, 2021). The wet deposition occurs through precipitation and is very low between 0–5 µg/m^2/year for most of Greenland, Siberia, and northern Canada (AMAP, 2021; Sproveiri et al., 2017).

Sampling Area

Three sampling sites were selected for fieldwork: one site on Disko Island and two sites in Disko Bay (Figure 2).

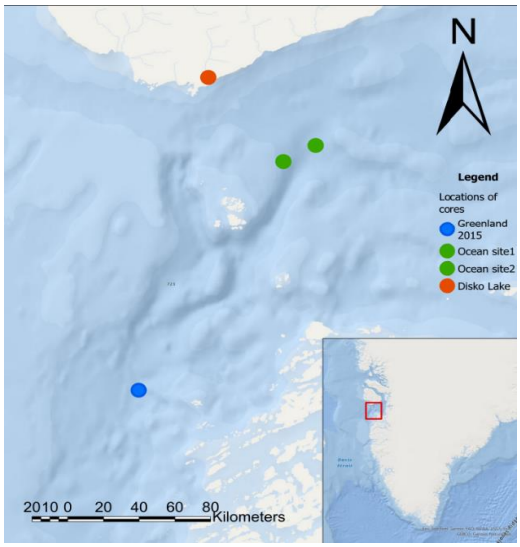

Figure 2: Location of sampling sites and the Greenland 2015 core that was used in the analysis.

Sampling sites 1 & 2: Diko Bay

The site is in Disko Bay on the west coast of Greenland. The area is a typical subarctic environment with frequent floating icebergs. Two locations were selected: one at 69°06.217' N, 53°05.815' W with a depth of 675 metres, and the other at 69°08.111' N, 52°56.070' W with a depth of 720 metres.

Sampling site 3: Disko Lake

The lake is located close to the southern coast of Disko Island, near the town of Qeqertarsuaq, at approximately 69°15′ N, 53°34′ W.

Sampling site: Greenland 2015

Due to complications of transportation, the sediment core samples taken on the Field Course 2024 could not be utilised. Therefore, the sediment samples used in this study are from a sediment core collected in 2015, referred to as ‘Greenland 2015’ which was sampled in Egedesminde Dyb at 68°38.888' N, 53°49.496' W at a depth of 870 m.

Methods

The methods used in this study include fieldwork, climate statistics, and analysis of the sediment samples to determine whether the mercury emissions are related to climate change. An overview is illustrated as a flowchart (Figure 3).

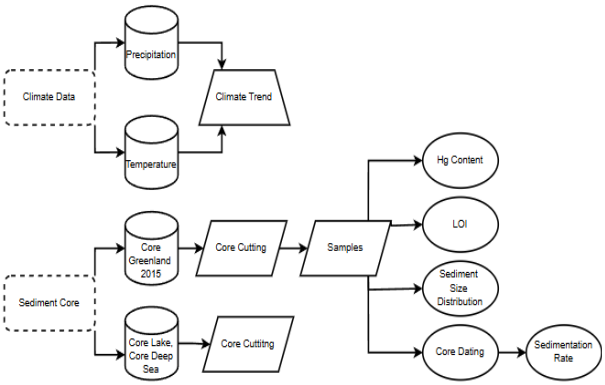

Figure 3: Flowchart showing the methods used.

Climate statistics

To investigate climate change and the relationship between climate change and mercury emissions, precipitation data from 1890 to 1984 and temperature data from 1840 to 2022 were sourced from The Danish Meteorological Institution (DMI, 2021). The data was processed in Rstudio and graphs were created for the annual temperature, average summer- and winter temperature, together with the accumulated winter- and summer precipitation.

Fieldwork and sample preparation

To analyse the mercury pollution, sediment cores were extracted in the Lake at Disko Island and in the deep sea at Egedesminde Dyb (Figure 2).

Lake on Disko Island

A suitable location in the lake was chosen based on bathymetry data collected through an echo sounder. Flat areas are ideal as the possibility of it being affected by sliding of sediments from surrounding areas is lower, which can change the chronological order of layers. The core was extracted with a kayak core at a suitable location or by manually pushing the tube through the lake bed.

Egedesminde Dyb in Disko Bay

With the ship Porsild, two suitable locations were found, where the seafloor was flat, and within a depth of ~700 m, as determined by an echo sounder, for the fieldwork sampling. The optimal depth was at the deepest spot in Egedesminde Dyb (~900 m), but due to a limited cable length of ~700 m, this was not accessible during the fieldwork. However, the core 'Greenland 2015', which was used for further analysis was extracted there at 870 m depth.

To extract the core, the coring device attached to the cable was released to the bottom of the sea and extracted when the tube had been partially submerged into the seafloor, in order to preserve the top of the core and thereby also preserving the chronological layering within.

Sample preparation

The sediment cores were cut in the laboratory, during this process a graphite knife (non-metallic) was used and all personal metal devices were removed. The water was removed from the cores with either suction through a hose or through draining them, when the tubes were cut just above the sediment to be transported whole to Denmark. Afterwards, the cores were placed on a core-extruder with 0.5 cm (lake) or 1.0 cm (sea) thick disks below it. To accurately separate layers, when the sediment was pushed up. The layers were stored in plastic bags. The 'Greenland 2015' core samples, which were used for the following analysis were in addition freeze-dried.

Sediment size distribution

To determine the sediment size at different depths, the Malvern Mastersizer 2000 Particle Analyser was used. 34 subsamples were extracted from the sediment core Greenland 2015 and combined with demineralised water and a "snaps" of sodium pyrophosphate 0.1 MOL. They were then dispersed for two minutes before they were added to the MALVERN particle analyser. The device determined the sediment size distribution by measuring the sizes 5 times with laser diffraction, before an average for each replicate was made.

Loss of ignition (LOI)

To find the organic content of the samples, the loss of ignition was determined. This was done with a subsample of the freeze-dried samples. The subsamples were first placed in a weighted crucible and dried in an oven at 105 °C for 1 hour, to remove any moisture which may have been present in the samples. The subsamples were then weighed and burned in a muffle furnace at 550 °C for two hours. The subsamples were subsequently removed from the furnace and weighed again. The difference in weight was used to calculate the LOI as described in equation 1.

$$\frac{(Dried\ sample\ weight - Burnt\ sample\ weight)}{Dried\ sample} * 100 \quad (1)$$

Dating with ^{210}Pb and ^{137}Cs

In order to evaluate the mercury content and correlate it to the climate data, the following method was used for the core Greenland 2015. The sediment core was dated with the Canberra ultralow-background Ge-detector which uses gamma spectrometry with isotopes from lead (Pb) and cesium (Cs). Gamma spectrometry using the isotope ^{210}Pb can be used to date sediment cores from the last 100-150 years, and with the isotope ^{137}Cs it is possible to date the last ~50 years (Álvarez-Iglesias et al, 2007).

^{210}Pb is used in gamma spectrometry, because of its suitable half-life time of 22.23 years (Pedrosa-García et al, 2020). The gamma spectrometry measures gamma rays emitted by ^{210}Pb through which it is possible to gain information about the activity of ^{210}Pb and thereby date the sample (Bonczyk, 2013). The results from Pb-dating were validated with the fall-out of the radionuclide ^{137}Cs that are released atmospherically as one of the products from nuclear fission (Andersen, 2017). By knowing when historical events occurred with nuclear fission, the date of the sediment could be defined by the detected values of ^{137}Cs (Kumar et al, 1999) e.g. from the Fukushima nuclear accident in March 2011 (Buesseler et al., 2011).

Total mercury

The total mercury was done by Jens Søndergård from Aarhus university. The analysis was conducted by using 0.5 g dry material dissolved with 5 ml aqua regia (3 part HCL and 1 part HNO_3) in 50 ml digitubes in a covered heating block at 95 °C for 2 hours. Afterwards the samples were diluted until they weighed 50 g with MilliQ water and analysed with an Agilent 7900 ICP-MS machine.

Results

Climate

The annual temperature on Disko Island in Greenland has increased by 0.0153 °C

every year from 1840 to 2022 (Figure 4) which is 2.78 °C in the given period. The minimum annual temperature occurred in 1863 at -8.9 °C and the maximum annual was in 2010 at 0.9 °C. Furthermore, the mean temperature for the summer and winter months both experienced an increase in temperature from 1840 to 2022 with a slope of 0.013 and 0.0275 °C respectively, which means that the temperature has increased 5.01 °C for the time period for winter and 2.33 °C for summer. The highest mean temperatures for summer- and winter months were 9.26 and -4.53 °C respectively and the lowest summer mean temperature was 3.03 °C and -22.73 °C for the winter mean temperature. Moreover, besides having the biggest increase per year, the winter temperature also has the highest variance compared to the annual and mean summer temperatures (Figure 4).

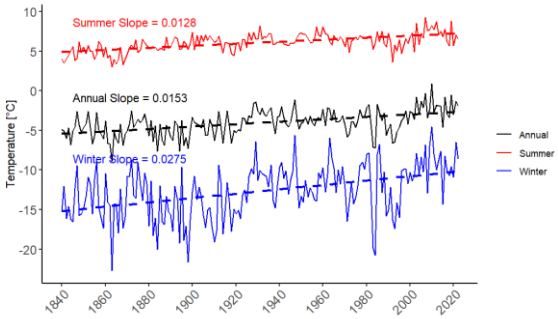

Figure 4: Annual temperature, and mean summer- (June, July & August) and winter (December, January & February) temperature for Disko Island from 1840 to 2022.

The precipitation measured in Ilulissat Greenland from 1890 to 1984 shows that the summer months received significantly more precipitation than the winter months (Figure 5). The highest amount of precipitation measured in the winter months was 163.5 mm in 1948 and 166 mm in 1942 for the summer months. The lowest precipitation falling in the winter months was 5.1 mm in 1934 and 15 mm in the summer months in 1943.

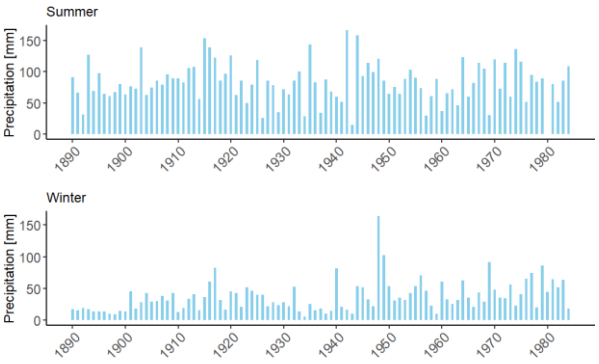

Figure 5: The sum of precipitation for Ilulissat from 1890 to 1984 for winter months (December, January &, February) and summer months (June, July, August) respectively. In the summer of 1980, there was no data. recorded, hence the gap in the figure.

Sediment size distribution

There is a pattern in the sediment distribution (Figure 6), as most curves peak at ~5.4-9.3 µm. The amount of large sediment sizes decrease with depth, as most of the top half (green) of the sediment core has a higher percentage of sediment sizes >49µm than the bottom half (red). The top 0.5 cm is different from the other layers, as it has a higher percentage of the sediment sizes ~7-8µm, and a lower percentage (>1%) of bigger sediment sizes >28 µm.

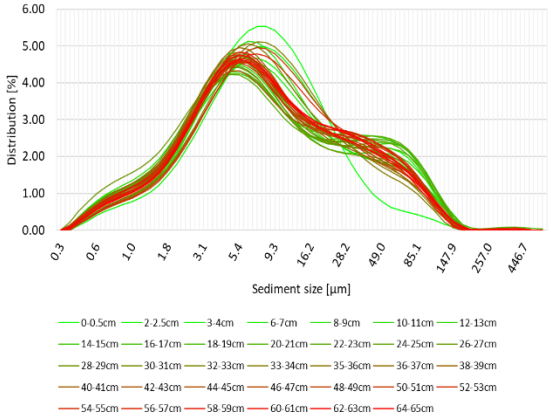

Figure 6: Sediment distribution curves that show how many percent the samples have of each sediment size.

The sediment distribution (Figure 6) shows that ~75-88% of the sediments in all depths consist of silt, which has sediment sizes between 2-63 µm. ~8-18 % of the sediment

consists of clay (<2µm), and the minority of the sediment consists of sand (>63µm) with values in the range of ~2-10 %. The top 0.5 cm of the sediment core consists of less sand than the rest of the core. The patterns of the silt content throughout the core show that the top 10 cm has a silt content >80%, 10-30 cm has <80% silt and most of 30-65 cm contains >80% silt.

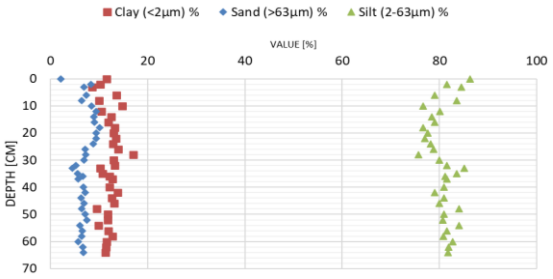

Figure 7. The amount [%] of sand, silt, and clay at different depths.

Loss of ignition (LOI)

The LOI which estimates the amount of organic content shows that in the first centimetre (0-1 cm) it has the highest measurements at 8.66 % and 8.19 %, at respectively 0-0.5 cm and 0.5-1 cm depth. From 1-38 cm depth, the values vary between 7-8 % LOI, with the exception of 23-24 cm depth where the lowest measure of LOI was 6.81 %. The bottom part of the sediment core from 38-66 cm depth, measured 6.9-7.3 % LOI, which was lower than most of the above sediments and had a smaller variability in LOI.

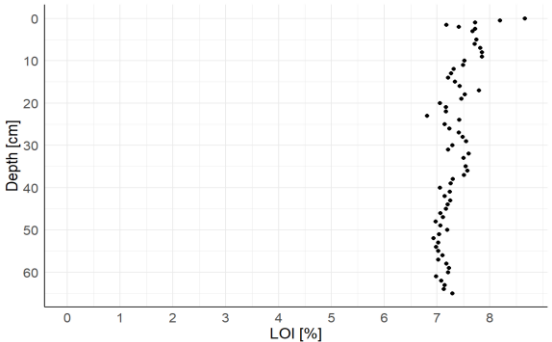

Figure 8: LOI [%] at different depths. The first 6 measurements have a 0.5 cm depth range while those from 4 - 68 are a depth range of 1 cm. There are no values for the depths 3-4 cm and 34-35 cm.

Sediment dating with Pb and Cs

The highest amount of lead is seen in the top layers of the core, whereas it then decreases with depth (Figure 9). The highest amount is ~450 bq kg-1 in a depth of 0.25 cm. The lowest is 2 bq kg-1 at a depth of 50 cm. The rate of increase of lead is higher at the top of the core compared to the bottom, where the samples in the first 10 cm have a lead level ranging from 250 to 450 bq kg-1. The samples for the last 15 cm have lead values close to 0. As the samples are not at consistent intervals, attention must be paid to observations. The gap between 40 and 50 cm is due to a large sample size from 40-49 cm.

Cesium only exists in the first 20 cm of the core (Figure 9), ranging from approximately 1.8 to 13.8 bq kg-1. Moreover, it has a relatively high variability with two peaks at ~12 and ~14 respectively.

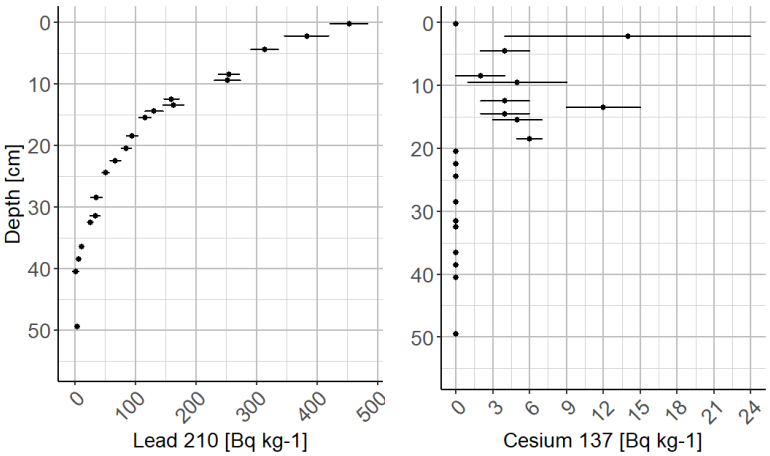

Figure 9: Raw data of Lead and Cesium levels at different depths in the sample core, with uncertainties represented as bars.

Total Mercury

An overview of the mercury content at the different depths is presented in Figure 10. A linear relationship is shown between the depth and mercury level with an R^2 value of 0.96. When mercury decreases by 1 µg/kg the depth decreases by 1.24 cm. Thus, the deeper the depth the lower the mercury content.

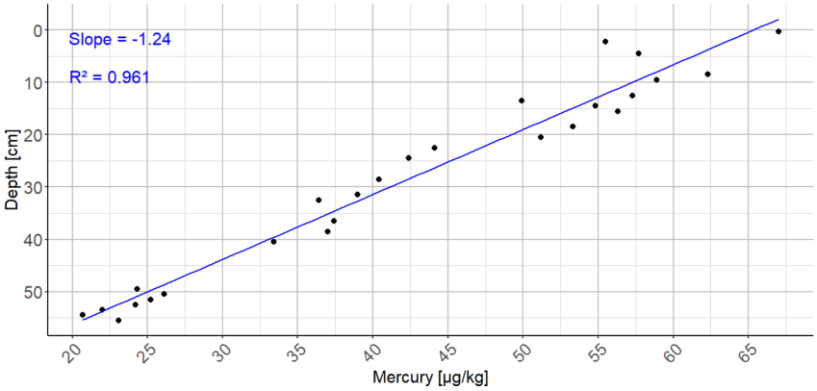

Figure 10: Mercury level at different depth in the sample core.

The total mercury measured appears to have a linear relationship with years with an R^2 value of 0.89 (Figure 11). Every year, mercury increases by 0.21 µg/kg. The mercury content was highest in 2014 at approximately 67 µg/kg and lowest in 1874 at approximately 33 µm/kg.

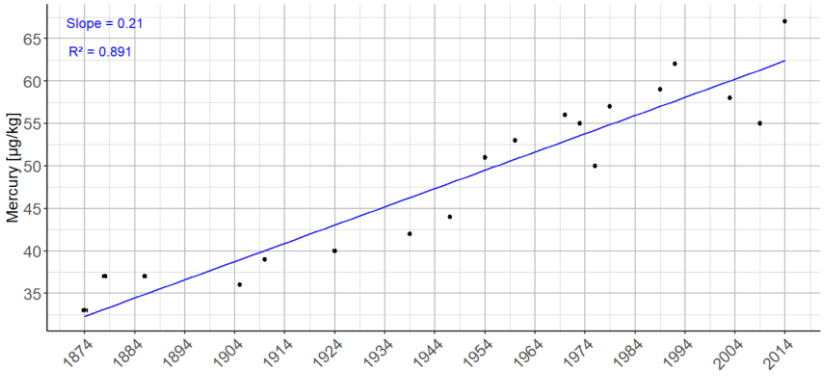

Figure 11: Mercury level at different years from the sample core.

The lead and cesium results were used for dating the Greenland 2015 core. Figure 12 presents an overview of the age at the different depths. The depth of 40 cm is from 1874, and the top of the core is from 2014. An almost linear relationship is shown between age and depth, when depth increases age decreases (getting older).

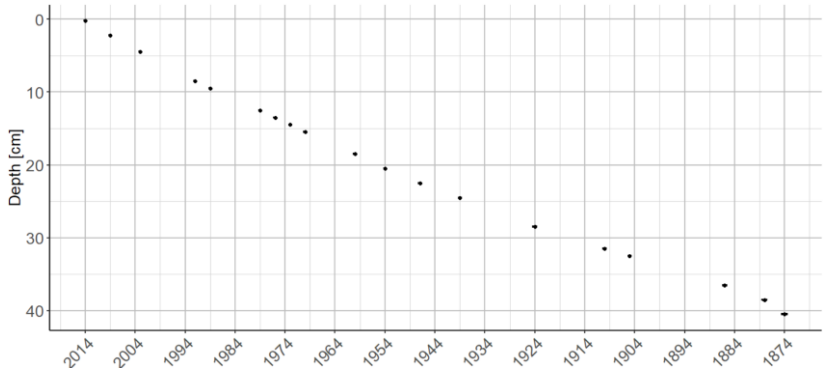

Figure 12: The years of the different depths in the sample core.

Sedimentation rate

The sedimentation rate for the Greenland 2015 sediment core was calculated for the top 40.5 cm to have an average sedimentation rate of 2.7 mm/year. In order to investigate the development of the sea

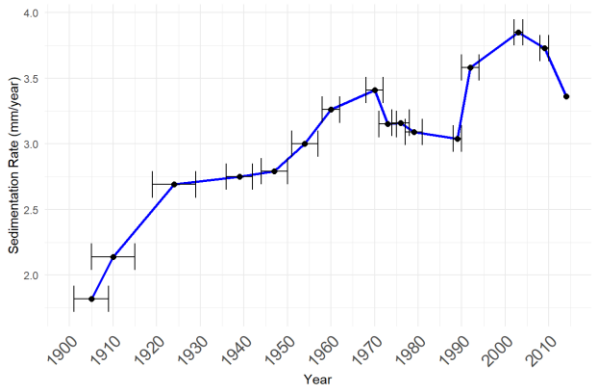

Figure 13: Sedimentation rate for the Greenland 2015 core over time.

floor the sedimentation rate over time was calculated (Figure 13). Sedimentation rate started to increased from 1.82 mm/year to 3.85 mm/year in the period 1905-2003. There was a slight drop and then an almost stable sedimentation rate in the 19 years from 1970-1989.

Discussion

Mercury

The mercury content was found to be highest in the top layer (>65 µg/kg) and decreased with depth to a value of <25 µg/kg below 50 cm. Overall there has been an increase in mercury through time from 1874-2014, and this clearly indicates that more mercury has been released into the atmosphere and deposited in Greenland at the location in Disko Bay. The increase in Figure 11 is illustrated linearly with a trend line. However, another interpretation could be that from previous to 1924 there was a slower deposition rate of mercury compared to 1924-2014, where a steeper increase in mercury deposition is observed. Bindler et al (2001) on the other hand measured the highest deposition of Mercury in the 1970's and 1980's. The mercury values of the Greenland 2015 core are in the range of the measured values of mercury in Greenland from the study by Asmund and Nielsen (2000), where 20 marine cores were extracted with values from 5 µg/kg to 250 µg/kg. Their results from a core in Disko Bay from 1994 at a depth of 221 m showed a value of 20 µg/kg, which is lower than the value we found from 1992 which was 62 µg/kg. This deviation could be due to the difference in depth and thus possible differences in grain sizes.

As 30 % of mercury originates from anthropogenic sources (and 60 % from re-release) (UN Environment, 2019), an increase in anthropogenic release could be an explanation for the increasing mercury content through time, especially after the industrialisation period that lasted from ~1850-1950.

Mercury and climate data

The climate data indicates that the largest increase is in the winter temperature from the period 1840-2020 (Figure 4). Binder et al (2001) emphasise that lakes closer to the Greenland Ice Sheet have been found to have a higher concentration of mercury than the ones further away. This could indicate that some of the mercury originates from the ice and that the increasing temperatures could lead to higher melt rates. Thus, there could be a correlation between the increased temperatures and higher content of mercury through time. However, to investigate the relationship between increasing temperature and higher mercury levels, a statistical test for significance would be needed.

The precipitation data shows a small increasing trend for the winter months and an irregular pattern in the summer months. However, a more distinct trend in precipitation was expected as well as a possible connection between this variable and mercury, as periods with more precipitation could have caused higher deposition rates of mercury to the soil. Moreover, as precipitation in the winter months is snowfall, mercury will be bound in the ice and snow, therefore it would not be re-released before the snow and ice melts. Therefore, the summer precipitation

is more interesting as this in most cases would be rainfall. However, it is important to note, that only the summer and winter months are being presented and therefore the precipitation for the other months is not included. Investigating all seasons could potentially have shown more distinct precipitation patterns.

Mercury and LOI

The observed organic content from the LOI was found to be highest in the top layer with a value of 8.7 %. The mercury content was also highest in the top layer, which is expected considering that mercury is bound to organic matter. However, as the mercury content decreases with depth the organic matter does not vary severely, even though the bottom half had a lower content of organic matter than the top half of the sediment core did. Thus, the variation in mercury content is not due to variations in the organic content alone.

Mercury and sediment size distribution

The sediment size distribution indicated that ~75-88 % of the sediment in all depths consisted of silt and that the top 0.5 centimetre had the highest silt content. Cohesion effects are high in clay due to the electrical attraction between the molecules and the small particle size of clay (Yin et al, 2021), which makes it easier for other particles to be bound to it. This could also be a contributing factor to the higher mercury content in the top layer, as it is easily bound to the clay molecules (Fernández-Martínez, 2019). However, as the core appears to have a high content of silt in all depths, it could be argued that high levels of mercury could have been found at all depths. As this is not the case, other factors need to be accounted for e.g. the concentration of anthropogenic mercury over time.

Mercury and sedimentation rate

As previously explained total mercury is observed to increase over time, and for most of the measured period, so has the sedimentation rate. If the mercury concentration in the atmosphere had remained constant, it would have been expected that an increase in sedimentation rate would have led to a decrease in mercury vertically in the core. This is due to the deposition rate of mercury staying the same but the increase in sedimentation rate removing the mercury deposition at a higher rate than previously. That is, however, not what is observed in this data as both the sedimentation rate and mercury concentration are observed to increase. Leading to the understanding that there has been an overall increase in mercury deposition from the atmosphere in the arctic region near Disko Bay. This is further supported by Asmund and Nielsen (2000) who also found that mercury deposition was higher in the samples from 1994 than those from 100 years previous and contributed that to anthropogenic input.

Conclusion

It can be concluded that there is a measured increase in mercury in the period 1874-2014. From the climate data, it can be concluded that there is an increase in temperature in the same period and that the winter temperature has had the highest increase (0.3 °C/year) compared to the annual- and summer temperature (0.2 °C/year and 0.1 °C/year). From the two results alone, a direct connection between the temperature increase and the increase in

mercury cannot be stated. However, the increase in temperature could be a contributing factor. Other parameters have been analysed in this study, and among these are the organic content through loss of ignition (LOI) and sediment size distribution. The results showed that the organic content was highest (8.7 % Carbon) in the top 1 cm of the sediment core (year 2014), which matches the year with the highest mercury value. The first centimetre also had the largest amount of fine-grained sediment, which mercury is easily bound to. Even though the organic matter content was highest in the top half of the sediment core (7-8.7 %) compared to the bottom half (6.9-7.3 %), it did not vary severely with depth and did not decrease linearly with depth as the mercury content did. It could therefore be a contributing factor for the mercury content but not the sole source. In addition, the sediment sizes distribution did not vary linearly with depth either.

None of the parameters researched in this study alone explains the increase in mercury. However, temperature increase, organic matter and higher fine-grained sediment content within the core are all contributing factors. The anthropogenic increase in released mercury during the last 150 years is also important to note.

Litterature

Álvarez-Iglesias, P., Quintana, B., Rubio, B., & Pérez-Arlucea, M. (2007). Sedimentation rates and trace metal input history in intertidal sediments from San Simón Bay (Ría de Vigo, NW Spain) derived from 210Pb and 137Cs chronology. Journal of Environmental Radioactivity, 98(3), 229–250. https://doi.org/10.1016/j.jenvrad.2007.05.001

AMAP Summary, (2021). AMAP Assessment 2021: Summery for policy-makers. Arctic Monitoring and Assessment Programme (AMAP), Tromsø, Norway.

AMAP, (2011). AMAP Assessment 2011: Mercury in the Arctic. Arctic Monitoring and Assessment Programme (AMAP), Oslo, Norway. xiv + 193pp.

AMAP, (2021). AMAP Assessment 2021: Mercury in the Arctic. Arctic Monitoring and Assessment Programme (AMAP), Tromsø, Norway. viii + 324pp

Andersen, T. J. (2017). Some Practical Considerations Regarding the Application of 210Pb and 137Cs Dating to Estuarine Sediments. In K. Weckström, K. M. Saunders, P. A. Gell, & C. G. Skilbeck (Eds.), Applications of Paleoenvironmental Techniques in Estuarine Studies (Vol. 20, pp. 121–140). Springer Netherlands. https://doi.org/10.1007/978-94-024-0990-1_6

Asmund, G., & Nielsen, S. (2000). Mercury in dated Greenland marine sediments. The Science of The Total Environment, 245(1–3), 61–72. https://doi.org/10.1016/S0048-9697(99)00433-7

Bindler, R., Renberg, I., Appleby, P. G., Anderson, N. J., & Rose, N. L. (2001). Mercury Accumulation Rates and Spatial Patterns in Lake Sediments from West Greenland: A Coast to Ice Margin Transect. Environmental Science & Technology, 35(9), 1736–1741. https://doi.org/10.1021/es0002868

Bonczyk, M. (2013). A Determination of the Concentration Level of Lead 210PB Isotope in Solid Samples for the Assessment of Radiation Risk Occuring in Coal Mines. Journal of Sustainable Mining,12(2),1–7. https://doi.org/10.7424/jsm130201

Buesseler, K., Aoyama, M., Fukasawa, M., (2011). Impacts of the Fukushima nuclear power plants on marine radioactivity. Environ. Sci. Technol. 45, 9931–9935. https://doi.org/10.1021/es202816c

Chouvelon, T., Strady, E., Harmelin-Vivien, M., Radakovitch, O., Brach-Papa, C., Crochet, S., Knoery, J., Rozuel, E., Thomas, B., Tronczynski, J., Chiffoleau, J.F., (2019). Patterns of trace metal bioaccumulation and trophic transfer in a phytoplankton-zooplankton-small pelagic fish marine food web. Mar. Pollut. Bull. 146, 1013–1030. https://doi.org/10.1016/j.marpolbul.2019.07.047.

DMI (2021). Greenland – DMI, Historical Climate Data, Collection 1784-2020 (DMI Report 21-04). Danish Meteorological Institute (DMI). https://www.dmi.dk/publikationer

Fernández-Martínez, R., Esbrí, J. M., Higueras, P., & Rucandio, I. (2019). Comparison of mercury distribution and mobility in soils affected by anthropogenic pollution around chloralkali plants and ancient mining sites. Science of The Total Environment, 671, 1066–1076. https://doi.org/10.1016/j.scitotenv.2019.03.348

Harding, G., Dalziel, J., Vass, P., (2018). Bioaccumulation of methylmercury within the marine food web of the outer Bay of Fundy, Gulf of Maine. PLoS ONE 13 (7), 1–30. https://doi.org/10.1371/journal.pone.0197220.

Horowitz, H. M., Jacob, D. J., Zhang, Y., Dibble, T. S., Slemr, F., Amos, H. M., Schmidt, J. A., Corbitt, E. S., Marais, E. A., & Sunderland, E. M. (2017). A new mechanism for atmospheric mercury redox chemistry: implications for the global mercury budget. Atmospheric Chemistry and Physics, 17(10), 6353–6371. https://doi.org/10.5194/acp-17-6353-2017

Jackson, T. A. (1998). Mercury in aquatic ecosystems. In W. J. Langston & M. J. Bebianno (Eds.), Metal Metabolism in Aquatic Environments (pp. 77–158). Springer US. https://doi.org/10.1007/978-1-4757-2761-6_5

Kumar, U. S., Navada, S. V., Rao, S. M., Nachiappan, Rm. P., Kumar, B., Krishnamoorthy, T. M., Jha, S. K., & Shukla, V. K. (1999). Determination of recent sedimentation rates and pattern in Lake Naini, India by 210Pb and 137Cs dating techniques. *Applied Radiation and Isotopes*, *51*(1), 97–105. https://doi.org/10.1016/S0969-8043(98)00148-1

Lindsey, R., & Dahlman, L. (2024). Climate Change: Global Temperature | NOAA Climate.gov. Climate Change: Global Temperature. http://www.climate.gov/news-features/understanding-climate/climate-change-global-temperature

Mason RP, Sheu GR. (2002). Role of the ocean in the global mercury cycle. Glob Biogeochem Cycles 2002;16:1093.

Masson-Delmotte, V., Swingedouw, D., Landais, A., Seidenkrantz, M., Gauthier, E., Bichet, V., Massa, C., Perren, B., Jomelli, V., Adalgeirsdottir, G., Hesselbjerg Christensen, J., Arneborg, J., Bhatt, U., Walker, D. A., Elberling, B., Gillet-Chaulet, F., Ritz, C., Gallée, H., Van Den Broeke, M., … Vinther, B. (2012). Greenland climate change: from the past to the future. WIREs Climate Change, 3(5), 427–449. https://doi.org/10.1002/wcc.186

McConnell, J.R., Edwards, R., (2008). Coal burning leaves toxic heavy metal legacy in the Arctic. Proc. Natl. Acad. Sci. U. S. A. 105 (34), 12140–12144. https://doi.org/10.1073/pnas.0803564105.

Pedrosa-García, M. C., Fontela, M., Quintana, B., Pérez, F., Francés, G., & Marcos, T. (2020). Precise 210Pb determination with high-efficiency gamma spectrometry for dating of marine sedimentary cores. Applied Radiation and Isotopes, 156, 108962. https://doi.org/10.1016/j.apradiso.2019.108962

Sprovieri, F., Pirrone, N., Bencardino, M., D'Amore, F., Angot, H., Barbante, C., Brunke, E.-G., Arcega-Cabrera, F., Cairns, W., Comero, S., Diéguez, M. D. C., Dommergue, A., Ebinghaus, R., Feng, X. B., Fu, X., Garcia, P. E., Gawlik, B. M., Hageström, U., Hansson, K., … Zhang, H. (2017). Five-year records of mercury wet deposition flux at GMOS sites in the Northern and Southern hemispheres. Atmospheric Chemistry and Physics, 17(4), 2689–2708. https://doi.org/10.5194/acp-17-2689-2017

Tovgaard, J. L., Westh, S. M., & Andersen, T. J. (2024). Historical flux of mercury to marine sediments in Sermilik Fjord and Young Sound, East Greenland (DRAFT).

UN Environment, (2019). Global Mercury Assessment 2018. UN Environment Programme, Chemicals and Health Branch Geneva, Switzerland

Westergaard-Nielsen, A., Hansen, B. U., Elberling, B., & Abermann, J. (2020). Greenland Climates. In Encyclopedia of the World's Biomes (pp. 539–550). Elsevier. https://doi.org/10.1016/B978-0-12-409548-9.11750-6

Yaqiong Mu, Yanqiang Wei, Jinkui Wu, Yongjian Ding, Donghui Shangguan, and Di Zeng (2020). Variations of Mass Balance of the Greenland Ice

Sheet from 2002 to 2019.Remote Sens. doi:10.3390/rs12162609

Yin, K., Fauchille, A.-L., Filippo, E., Kotronis, P., & Sciarra, G. (2021). A Review of Sand–Clay Mixture and Soil–Structure Interface Direct Shear Test. Geotechnics, 1, 260–306. https://doi.org/10.3390/geotechnics1020014

Greenhouse Gas Fluxes & Carbon Budget in the Foreland of Lyngmarksbræen

Halby, Simon B., Nørskov-Lauritsen, Svend*, Rude, Casper H.*, Strøbæk, Ditte**

**Cand.Scient.Stud.Geog. Geography & Geoinformatics, Department of Geoscience and Natural Resource Management, University of Copenhagen, Denmark, Øster Voldgade 10, 1350 København*

Abstract. Studies of carbon budget and greenhouse gas (GHG) fluxes are essential to better understand climate change. This project uses field measurements of CO_2, CH_4, and N_2O fluxes and analyses carbon content in the soil of the foreland of Lyngmarksbræen, a retreating glacier located on the island of Disko. Satellite imagery is used to calculate the area and age of newly exposed soil using normalized difference snow index (NDSI). The flux results show that the glacier foreland acts as a source of CO_2 and CH_4, while functioning as a sink for N_2O fluxes. The total CO_2-eq budget from exposed soils since 1985 was estimated to be 7.910 or 20.831 tons of CO_2-eq, depending on the glacial retreat model used, which corresponds to 2.157 / 5.681 tons of carbon emissions. No trend was found when comparing the measurement sites CO_2-eq fluxes with distance to the glacier. Carbon pool analysis revealed that the soils sequestered 2.464 / 6.489 tons of carbon during the same period, leading to a net carbon sink of 307 / 808 tons carbon since 1985. No trend was found for the amount of carbon stored in the soil and the age of the soil.

Introduction

The cryosphere plays an essential role in the world's climate system and has an impact on the surface energy budget, the water cycle, primary productivity, sea level and surface gas exchange (IPCC, 2013). Glaciers are key indicators of climate

change, and as a consequence of increasing temperatures, a general deglaciation is observed (Paul et al., 2016; Yao et al., 2020). Txhe changes in temperature are especially increasing in the arctic region, which has seen warming four times faster than the rest of the globe since 1980 (Rantanen et al., 2022). Peripheral glaciers and icecaps in Greenland have in recent decades undergone significant mass loss in response to climate change, with surface temperatures increasing between ~1.7 °C (summer) and ~4.4 °C (winter) in the period from 1991 to 2019 (Gillespie, 2023).

As glaciers retreat, they unveil vast areas of previously ice-covered terrain. These areas become relevant in the context of global greenhouse gas cycling, as they can either act as sources or sinks of greenhouse gases (Virkkala et al., 2024). In this project the gases carbon dioxide (CO_2), methane (CH_4), and nitrous oxide (N_2O) will be the focused GHG. However, the net contribution of these gases to the atmosphere from glacier foreland soils remains uncertain, especially as soil properties, microbial communities, and climate factors interplay to influence gas fluxes (Serrano-Silva et al., 2014). Recent evidence suggests that these soils can accumulate carbon over time, potentially functioning as long-term carbon sinks (Kabala, 2012; Huang, 2023)

This project addresses the knowledge gap by investigating both the greenhouse gas emissions and carbon storage in the foreland of Lyngmarksbræen, a retreating glacier in western Greenland. Specifically, the study focuses on assessing the fluxes of CO_2, CH_4, and N_2O, while also evaluating the carbon pools within the exposed soil to provide a more complete picture of its role in the global carbon cycle.

By combining field measurements and remote sensing techniques, this project aims to quantify the carbon budget for all the soil that has been exposed since 1985, due to deglaciation at the Lyngmarksbræen. The area of the glacier will be estimated using Sentinel and Landsat satellite images, to calculate an annual change in the glacial extent. By combining the CO_2 equivalent fluxes and carbon pool estimates from the glacier foreland soil, the total carbon budget in the area exposed since 1985 will be calculated, providing a comprehensive carbon budget for these newly exposed soils.

Study Area

North of the town Qeqertarsuaq, located on the Disko Island off the western coast of Greenland, is the Lyngmark mountain. On the top of the mountain is an Ice cap, Lyngmarksbræen, with 6 outlet glaciers (Gillespie, 2023). Our remote sensing analysis estimates Lyngmarkbræen to be 21 km^2 in 2021. The fieldwork for this project was conducted at the southern extent of Lyngmarkbræen. An overview of the area can be seen in figure 1.

The fieldtrip to Lyngmarks mountain was done on the 26th of August. The air temperature was 6°C at the arctic station in Qeqertarsuaq, whilst it was between ~ -1°C and ~2°C at the mountain. We experienced an elevation gain of 881 m during our trip, although according to Gillespie (2023) Lyngmarkbræen spans from ~425 m and ~950 meters above sea level.

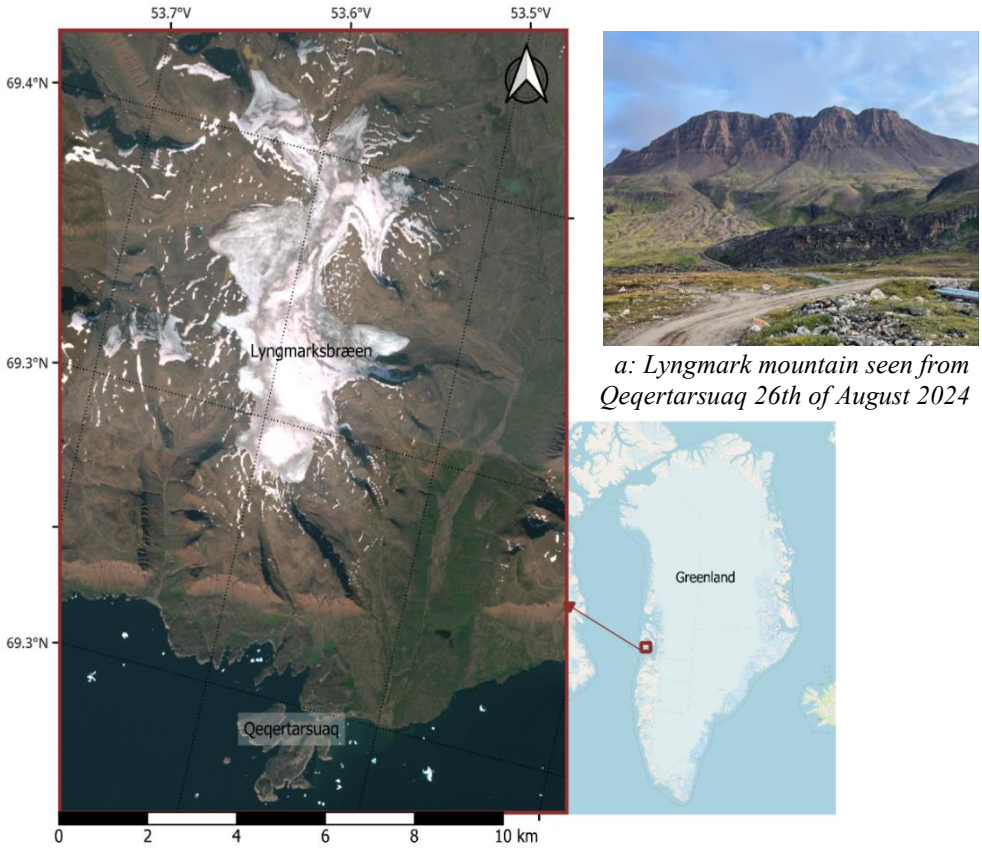

a: Lyngmark mountain seen from Qeqertarsuaq 26th of August 2024

Figure 1: The study area: Lyngmarksbræen and a) Lyngmark mountain in west Greenland

Theory

Soil is an important component in the global greenhouse gas balance and can act both as a sink and source for the investigated greenhouse gasses: CO_2, CH_4 and N_2O (Virkkala, 2024). The flux of these gases between soil and atmosphere is driven by biological and chemical processes which depend on soil properties, microbial activity, moisture content and temperature. The following section will outline the primary processes in soil that contribute to CO_2, CH_4 and N_2O fluxes.

Greenhouse Gas (GHG) Fluxes

The fluxes of CO_2, CH_4, and N_2O in soils are driven by various biological and chemical processes.

CO_2 is primarily released through soil respiration, where microorganisms decompose organic matter, with rates influenced by soil organic matter, temperature, and moisture (Phillips et al., 2015). CH_4 emissions are controlled by the balance between methanogenesis, an anaerobic process that produces methane, and methanotrophy, where methane is oxidized in aerobic conditions (Serrano-Silva et al, 2014).

N_2O is produced during nitrification and denitrification, microbial processes driven by nitrogen availability (Barnard et al, 2004). Nitrification occurs in oxygen-rich soils, while denitrification dominates in oxygen-poor, saturated soils, both contributing to N_2O emissions.

Carbon Pools

Carbon pools refer to the reservoirs of carbon stored in the Earth's systems, including the atmosphere, oceans, vegetations and soil. Carbon pools play a crucial role in regulating the global carbon cycle (Dheri, 2021). This section will focus on soil carbon pools in arctic areas near retreating glaciers.

Soils near retreating glaciers present unique challenges for carbon storage. The cold temperature and slow decomposition rates allow significant carbon accumulation over longer time periods (Huang, 2023). However, as glaciers retreat and expose new soils, these soils initially have extremely low to no carbon content because of the lack of organic input. Over time, vegetation will emerge and store carbon from the atmosphere into the soil (ibid.). As a result, newly exposed soil can act as carbon sinks. However, this balance is dependent on a lot of parameters, as mentioned in the section above (ibid).

Methods

This report applies a range of methods, incorporating satellite data, gas flux measurements, and soil carbon content analysis. Each of these methods is detailed in the following sections.

Estimating the Area of the Glacier

Initially the ice extent on the southern part of Lyngmarksbræen was outlined through manual delineation for six different years. The six glacial extents, along with a transect of six points were established for field sampling and measurements and can be seen in Figure A.1 in the appendix. These delineations were not used further in this paper, as they were time consuming and were based on subjective evaluation of snow, ice and soil.

To estimate the entire area of Lyngmarksbræen, a Normalized Difference Snow Index (NDSI) is used, which is a common method to identify snow and ice cover on optical images (USGS, 2024). NDSI is calculated by using two spectral bands: the green and the shortwave infrared (SWIR) band. NDSI can be calculated based on equation 1:

$$NDSI = \frac{(Green - SWIR)}{(Green + SWIR)} \qquad (1)$$

This method exploits snow and ice's optical signature, characterized by high reflectance in the green wavelengths and low reflectance in the SWIR wavelengths. For each image, the NDSI was calculated using the specified band for the satellite. A threshold value of 0.2 NDSI was chosen to classify the presence of snow or ice. This threshold was chosen based on Paul et al., (2016). The total area covered by snow or ice was subsequently calculated by summing the pixels with NDSI values equal to or greater than the threshold for each year. The data was obtained from Landsat and Sentinel as presented in Table 1.

Based on the calculated extent of the glacier, an average exposure time of the soil was calculated based on the distance from the 1985 extent to the 2021 extent. Here a distance of 588 meters was found. This gives a yearly retrieval rate of 16 meters pr. year. Based on the distance from the 1985 extent, an average exposure time of the soil at each site can be found in years. The age and the year of exposure is presented in Table 2. This gives an average amount of exposure of 16 years, which will be further

used to calculate the yearly carbon absorption by the soil.

Soil Samples and Fluxes

In situ measurements of CO_2, N_2O and CH_4 fluxes between the soil and atmosphere were recorded on August 26, 2024, at three sites (M1-M3), with three replicas (L1, L2 and L3). Soil samples were done for five sites (M1-M5) obtained at two depths (D1 and D2), with three replicas per depth (R1, R2, and R3). The in situ measurements and soil samples follow the transect along the glacier's retreat based on the manual delineation. M1 represents the most recent exposure (2021) and M5 the longest-exposed soil. M1-M5 was of loamy character. Additionally, M6 representing gravel-covered soil and M7 representing vegetated soil were collected, but not further used in the analysis.

In situ gas flux measurement was conducted using two different instruments, one for N_2O and one for CH_4. A chamber was placed on plastic collars for each measurement location (Figure 2) and the measurements were conducted for 4 - 10 minutes. The instruments employed operate by measuring gas concentrations within the chamber. The start to the end of the measurement period, were noted for later extraction of flux data. This allows for the calculation of emissions from the surface.

This is possible by utilizing knowledge of the chamber's volume and the height of the plastic collar. Furthermore, a fan within the chamber ensures an even distribution of air masses to avoid measuring errors of the concentrations. Due to weather challenges in the field, the gas chamber instrument for CH_4 malfunctioned after in situ measurement of M3, why no further in situ measurements was taken after site M3 for all gases. The final calculation of the in situ fluxes was created utilizing MATLAB script from Eckhardt and Kutzbach (2016). For each measurement, the start and ending time was modified to filter outliers and noise in data, to create a recalculated flux.

Table 1: Satellite data used to find the extent of the glacier, the source and the spatial resolution.

Years in August or September	Source	Resolution (m)
1979, 1985, 1995, 2000	Landsat	30
2017, 2019, 2021	Sentinel	20

Table 2: The distance from the 1985 extent and the calculated age. The calculated age is based on an annual retrieval rate of 16 meters pr. year.

Site	Distance from 1985 extent (m)	Exposure time of the soil (years since 2024)	Year exposed
M1	438	12	2012
M2	405	14	2010
M3	303	20	2004

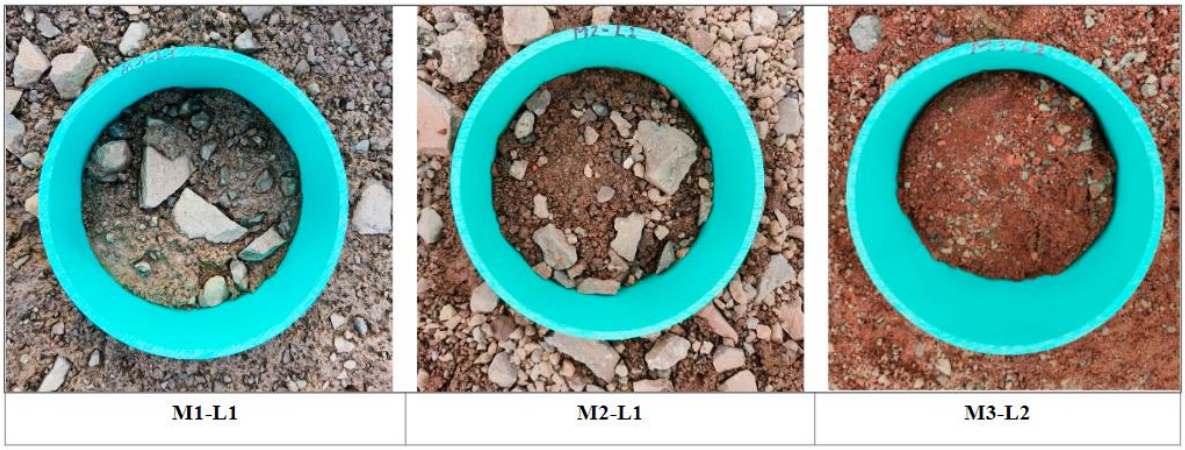

Figure 2: Example of the three sites for the flux measurements

Calculation of Carbon Pools

The soil samples taken were coated with parafilm after they were extracted in order to maintain the composition of the soil. All the samples were put in the fridge for 24 hours to imitate the temperatures in the ground. The sample was weighed with, and without, the ring, stones < 2 mm were filtered out and weighted and the volume was found. Hereafter a subsample was taken and transported to Copenhagen. Here ~5g was taken out and put in the oven for 24 hours and the water content was found. Finally, a small part of the samples where grinted and a C/N analysis was made to find the carbon content.

The calculation of soil carbon pool requires knowledge of the soil bulk density, carbon content and the depth of the sampled soil. The calculation of soil bulk density (BD) is based on the dry soil which is divided by the volume of the soil core. The carbon content (%C) is determined by laboratory analysis. Finally, the depth of each sampled soil is defined as 4 centimeters. When all variables are available, equation (2) is applied to calculate the carbon pool in the soil:

$$Carbon\,pool\,(gC/cm^2) = BD(g/cm^3) \cdot Total\,C\,(\%) \cdot Depth\,(cm) \quad (2)$$

The carbon pool is calculated for M1-M3. To ensure comparability, M4 and M5 were not part of the calculations, as in situ measurements were only available for M1-M3. No correlation between distance from the glacier and size of the carbon pool was identified, why an average carbon pool was applied for the whole study area. To estimate the yearly uptake of carbon by the soil, the calculated average carbon pool value was divided by the average exposure time in years, which was described in the previous section of *Estimating the Area of the Glacier.*

Upscaling

CO_2, CH_4, and N_2O fluxes is converted to CO_2-eq to account for the varying global warming potentials (GWP) of each gas - where CH_4 has a GWP of 25, and N_2O has 265 (Ritchie, 2020). The total GWP at each site is calculated to evaluate the fluxes contribution to local carbon budget.

The annual glacial retreat, found using NDSI, was used along with the in situ flux measurements to estimate the amount of greenhouse gases released from all the

newly exposed soil. To do so, an average of the CO_2-eq flux was found, as no changes along the glacier transect of the three points was found.

Now that an annual glacial retreat and a fixed annual CO_2-eq flux have been found, it is possible to determine the size of the CO_2-eq fluxes that the exposed soil releases. First, the accumulated size of fluxes from each year is calculated. This is done using equation 3.

$$AF_i = \bar{f} \cdot (2022 - x_i) \qquad (3)$$

Where x_i is the year of calculation, $\bar{f}$ is the average flux in μg CO_2-eq s^{-1} m^{-2} and *AF* is the Accumulated Flux. As the unit for AF is μg CO_2-eq s^{-1} m^{-2}, the AF for the whole exposed area can be found using equation 4.

$$AFA_i = AF_i \cdot AGR \cdot 10^6 \qquad (4)$$

Where *AFA* is the Accumulated Flux for the whole exposed Area and *AGR* is the annual glacial retreat, this varies whether 1979 is

used in the calculations of annual glacial retreat. The *AGR* is multiplied with 10^6 to convert the exposed area from km^2 into m^2. The amount of μg CO_2 s^{-1} has now been found for the soil, exposed in that given year, and the total amount of μg CO_2 for the whole season of two months can be found by using equation 5.

$$AFAS_i = AFA_i \cdot 60d \cdot 24h \cdot 3600s \quad (5)$$

Where AFAS is the Accumulated Flux for the whole exposed Area during the season of 2 months. Finally, the AFAS for each year can be found, summarized and converted into tons by using equation 6.

$$TAFS = \sum_{i=1}^{n} AFAS_i \cdot 10^{-12} \qquad (6)$$

Where TAFS is the Total Accumulated Flux from all the exposed Soil since 1985 in tons.

Results

The results for this project are presented in the following section.

Glacier Retrieval Rate

The historical extent of the glacier can be seen in Figure 3 and the calculated retrieval rate of the glacier can be seen in Figure 4. This shows an annual retrieval rate of 0.7 km^2 and 0.27 km^2 calculated with and without the extent from 1979 respectively.

Fluxes

The average N_2O, CO_2 and CH_4 fluxes for each site's replicas was calculated and is presented in Figure 5. This shows that the soils act as a sink for N_2O, and that the flux into the ground increases the further away from the glacier the site is located. The opposite can be seen with CH_4, which shows that the soil acts as a source of CH_4 to the atmosphere, and that the flux decreases the further away the site is located from the glacier. CO_2 shows a relatively high emission close to the glacier, then a low emission and then a high emission, away from the glacier. All but one flux (M2 CO_2) has very large standard deviations. Multiple of the standard deviations are larger than the flux itself. This shows that there were big variations between the replicas.

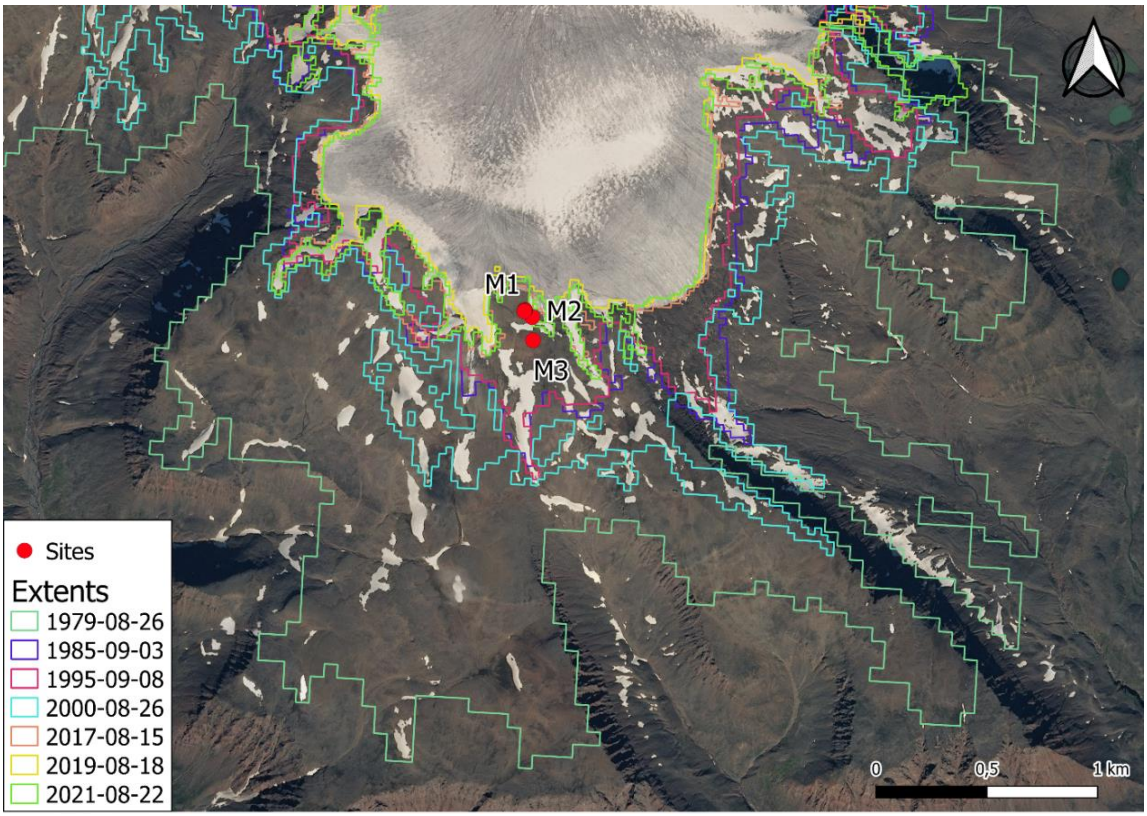

Figure 3. The sampling sites and the calculated extent of the glacier based on NDSI.

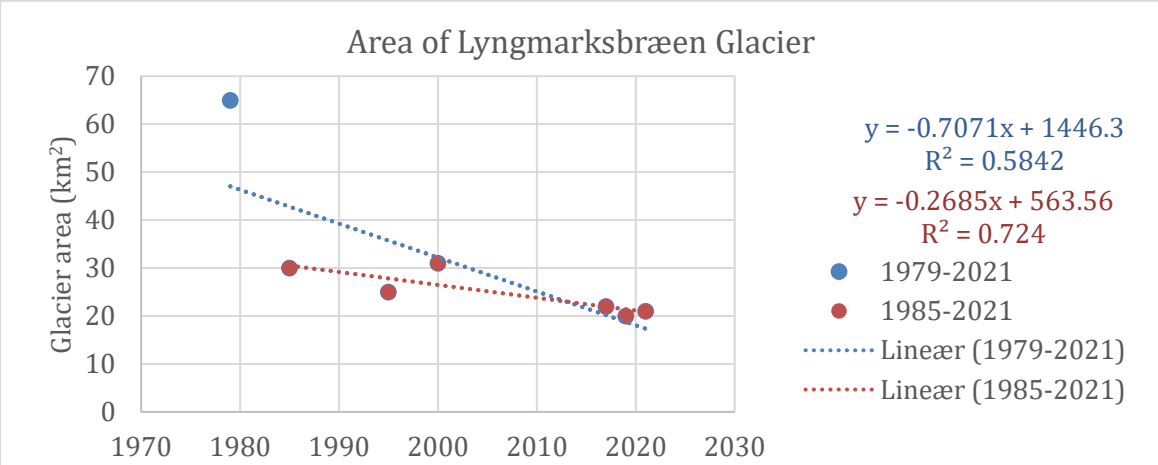

Figure 4. The area of the glacier and the calculated trend. The red dots and trendline represent calculated extents of the glacier based on NDSI without the 1979 observation. The blue colored dots and trendline use the same values, but also use the 1979 observation.

The fluxes for N_2O and CH_4 were converted into CO_2-eq and these are summarized with the CO_2 fluxes for each site, which can be seen in Figure 6. This shows that the main driver of greenhouse gas fluxes is CO_2.

When the three greenhouse gases are converted into CO_2-eq and summarized, they do not show any significant trend. This is largely due to the fact that no trend is seen in the CO_2 fluxes as the CO_2 fluxes account for the majority of the GHG fluxes. Since

no apparent trend is seen, the average of the three total CO_2 eq are calculated and found to be 8,1 µg CO_2 s^{-1} m^{-2}. This value will be assumed to represent all soils that have been exposed due to the retreating glacier.

Based on these retrieval rates and the calculated CO_2-eq fluxes, a total CO_2-eq budget for all soil exposed since 1985 has been calculated to be 20.831 tons and 7.910 tons when using the 1979-2021 and 1985-2021 glacier retrieval rate respectively. This can be converted into a value of 5681 ton C and 2157 ton C by using the weight relationship of C and CO_2 ($12\ \frac{g}{mol}$/ $44\frac{g}{mol}$).

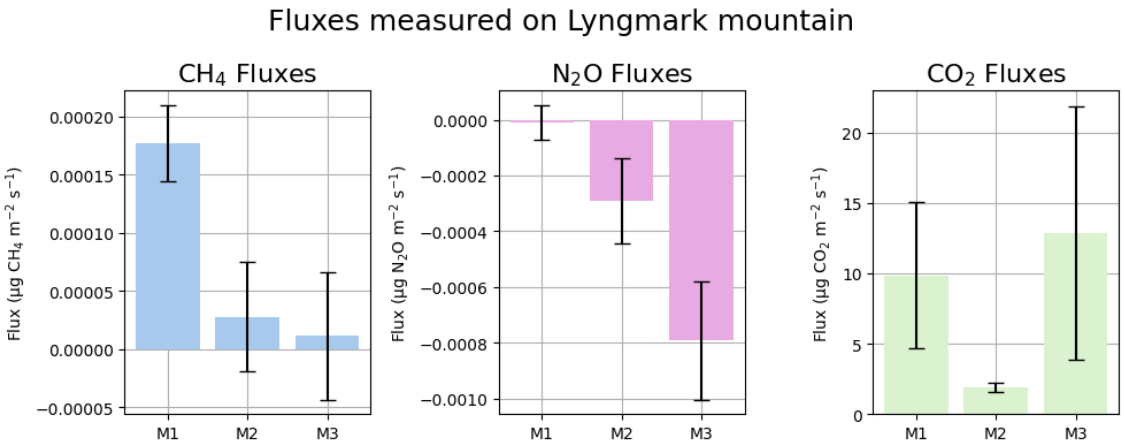

Figure 5. The three different fluxes for each site

	M1	M2	M3
CH_4 In CO_2-eq	0.00496	0.00078	0.00032
N_2O In CO_2-eq	-0.002694	-0.16402	-0.20959
CO_2	9.86235	1.87517	12.88332
Total CO_2-eq [µg CO_2 s^{-1} m^{-2}]	**9.86462** +/-	**1.71192** +/-	**12.67405** +/-

Figure 6. The fluxes for each site in CO_2 equivalents.

Carbon Pool Results

Figure 7 illustrates the carbon pools for each site (M1-M3). The calculations are based on the method presented in the *Carbon Pools* section. The carbon pools vary from 0.29 to 0.10 kgC/m^2. No significant correlation was identified between the carbon pool and distance from the glacier, as the theory otherwise suggests. For this reason, a mean value for all the sites was calculated, resulting in a value of 0.209 kgC/m^2 for the area.

The mean value of 0.209 kgC/m^2 was divided by the mean time of exposure (16 years), resulting in a yearly storage of carbon of 0.013 kgC/m^2/year.

To calculate how many tons carbon is stored in the newly exposed soil, the yearly storage of carbon is converted into ton carbon for the 1985-2021 period, calculated based on the soil's age. This results in 2464- and 6489-tons carbon stored in the soil, depending on the glacial retreat rate (with or without the 1979 extent).

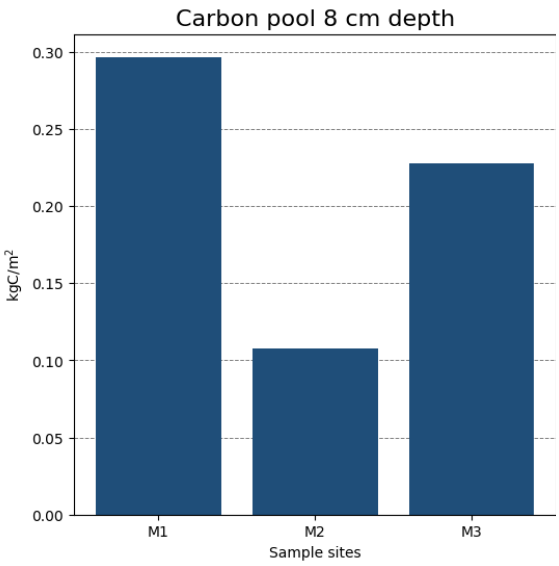

Figure 7. Overview of the carbon pool across the transect in kg C/m2 for 8 cm depth.

Final Calculation of Source vs. Sink

Based on the results from the previous sections, a final calculation can be made to determine the full extent of the carbon budget. This can be seen in Table 3. Based on the data in Table 3 it is clear that the soil acts as a sink for carbon, absorbing 306 / 807 ton C during the period of 37 years.

Table 3. The overall carbon budget for all the soil that has been exposed since 1985.

	Carbon pool (ton C)	Flux (ton C)	Total difference (ton C)
Glacier retrieval rate without 1979	2464	2157	307
Glacier retrieval rate with 1979	6489	5681	808

Discussion

Data Limitations in Estimating Glacier Extent

The delineation of Lyngmarksbræen is based on satellite images with varying spatial resolutions, which affect the accuracy of the glacier's boundaries. The selected years were selected based on two main criteria: Cloud free images and minimal snow cover. The dates of the images were limited to August or September as this was closest to the period of fieldwork.

High-resolution images would have resulted in more precise mapping compared to the 30-meter resolution of Landsat images from 1979, 1985, 1995, and 2000. Lower-resolution images lead to more generalized outlines of the glacier, making it difficult to detect smaller, newly exposed areas (Pope et al., 2014). This variability in resolution introduces uncertainty in determining the exact timeline of glacier retreat, as smaller changes may not be accurately captured.

Even with focus on finding images with minimal snow cover, differentiating between seasonal snow from permanent ice was a challenge. Located between ~425 m and ~950 meters above sea level, Lyngmarksbræen experiences significant snowfall, which can obscure the true extent of the glacier.

The use of the NDSI adds another layer of complexity. While NDSI effectively identifies areas of snow and ice by comparing green and SWIR reflectance, both snow and ice share similar spectral properties. The applied threshold of 0.2 proposed by Paul et al., (2016) could have been altered according to our data, to find a more accurate difference between glacier ice and snow in our study area, leading to less classification errors. Pope et al., (2014) mentions that snow has a higher reflectance in the SWIR than ice. Applying a different thresholds for each optical satellite image, based on for example precipitation data, could perhaps yield a more precise result. However, even if adjusting the threshold gave better accuracy it does not fully resolve the issue, particularly when using lower-resolution images.

Fieldwork Challenges

At the time of the fieldwork, Lyngmarks mountain was partially covered in new snow, limiting the ability to sample soil and measure gas fluxes at the intended pre-selected sites. Therefore, samples were taken on patches of ground with no snow cover as close to the pre-selected points as possible.

As mentioned in the method section, weather challenges caused a lack of in situ measurements at sites M4 and M5, which may affect the accuracy of CO_2 equivalent upscaling. Had the upscaling included data from the two additional sites, a better representation could have been achieved. In general, more frequent flux measurements and soil samples across multiple sites would provide a more representative average and perhaps shown tendencies. E.g. M3, the last in situ measurement, is located ~850 m away from the final extent of 1979, creating a relatively large data gap. Completing in situ measurements at all five sites could provide a more comprehensive dataset, enabling a possible detection of a trendline in the fluxes. A clear trend would improve the accuracy of the upscaling by utilizing flux values that reflect the varying

exposure times of the soil, rather than relying on a single average. This would also make it possible to investigate whether areas with longer exposure act as sources or sinks for different gases.

The assumption that fluxes occur for 60 days during summer when snow cover is minimal may introduce errors. Snow was still present near the glacier, potentially affecting local gas fluxes. Snow may insulate the ground, enhancing microbial activity and increasing fluxes, or on the contrary act as a physical barrier, reducing microbial activity (Xue et al, 2020). Future studies should analyze soil beneath snow cover to better understand gas flux dynamics.

Additionally, the replica selected was within a fairly restricted areas of snow-free patches, which leaves a portion of the soil type 'unknown' due to snow cover. At the first site, M1, vegetation and gravel were identified, where the flux was measured and soil samples collected (figure A.2). Had these soil types been included in the percentage they cover of the study area, a more representative result would have been possible.

Source or Sink

The results from our field measurements of fluxes and soil samples indicate that the area is a total carbon sink. However, when examining the methodology used for these calculations, it becomes clear that several sources of error may be present.

Firstly, the values of 5.681- and 2.157 ton C equivalents are based on 27 point flux measurements lasting around 5-10 minutes. This will inevitably give a large uncertainty when upscaling from one point to a greater area and from seconds to years. The same is evident for the soil samples, which also are extrapolated from single points into a larger area. Furthermore, a specific carbon pool value or flux from each site, instead of an average, would have resulted in a higher precision of the upscaling.

Throughout the entire investigation period, a total of 807 and 306 tons of carbon was absorbed, indicating an area with little carbon absorption capacity. For context the total sink is roughly equivalent to the annual emissions of about 646 and 245 passenger vehicles respectively (EPA, 2024).

Since the results show only a small carbon sink, the potential sources of error could significantly influence the final classification of the area as either a carbon source or sink. It is essential to consider these uncertainties when interpreting the findings.

Typically, it is expected to see an increase in the carbon pool with greater distance from the current ice extent (Thomazini et al, 2015). However, this trend was not clearly observed in the results. A unique source / sink calculation for each site could provide interesting insights into the tendencies as well of the complexity of soil sink and source properties along the transect. Ultimately, the reliability of the results is only as strong as the accuracy of the underlying measurements, which must be considered when evaluating these findings.

Upon examining the flux data for CO_2, a pattern is observed where high values are followed by low values, and then high values again. A possible explanation for this could be specific conditions at the sites that influence the final flux measurements. Near the glacier at M1, more water is

expected, which accounts for the larger flux values, while M2 shows lower flux possibly due to a smaller water quantity. Similarly, high values are observed at M3, which could be explained by a longer exposure time resulting in more developing soils, resulting in greater flux. This explanation needs much further investigation and information about the locally environment conditions, underlining the complicity of fluxes in the pro-glacial area.

Conclusion

This study concludes that the foreland of the retreating Lyngmarksbræen glacier contributes to greenhouse gas emissions through CO_2 and CH_4, while acting as a net sink for N_2O. The total CO_2 equivalent budget from the exposed soils since 1985 was found to be 7.910 / 20.831 tons of CO_2-eq, depending on the glacier retreat model used. When converted to C, these values correspond to a value of 2.157 / 5.681 tons of carbon emissions. The carbon pool analysis revealed that the soils have sequestered 2.464 / 6.489 tons of carbon during this period, resulting in a net carbon absorption of 306 / 807 tons. Despite high variability in fluxes, the lack of a trend in CO_2-eq fluxes and carbon content, highlights the complexity of greenhouse gas dynamics in newly exposed soils. These findings underscore the importance of accounting for both GHG fluxes and carbon storage in deglaciated landscapes when assessing their role in the global carbon budget. Future studies should focus on long-term monitoring to better capture seasonal variations and improve the understanding of carbon dynamics in these rapidly changing environments.

References

Barnard, R., Leadley, P.W. and Hungate, B.A., 2005. Global change, nitrification, and denitrification: A review. *Global Biogeochemical Cycles*, 19, GB1007. https://doi.org/10.1029/2004GB002282.

Dheri, G.S. and Nazir, G., 2021. A review on carbon pools and sequestration as influenced by long-term management practices in a rice–wheat cropping system. *Carbon Management*, 12(5), pp.559-580.. https://doi.org/10.1080/17583004.2021.1976674

EPA (2023) *Greenhouse Gas Emissions from a Typical Passenger Vehicle*. https://www.epa.gov/greenvehicles/greenhouse-gas-emissions-typical-passenger-vehicle (Accessed: 23 October 2024).

Gillespie, M.K., Yde, J.C., Andresen, M.S., Citterio, M. and Gillespie, M.A.K., 2023. Ice geometry and thermal regime of Lyngmarksbræen Ice Cap, West Greenland. *Journal of Glaciology*, pp.1-13. https://doi.org/10.1017/jog.2023.89

Kabala, C. and Zapart, J., 2012. Initial soil development and carbon accumulation on moraines of the rapidly retreating Werenskiold Glacier, SW Spitsbergen, Svalbard archipelago. *Geoderma*, 175-176, pp.9-20. https://doi.org/10.1016/j.geoderma.2012.01.025

Paul, F., Winsvold, S.H., Kääb, A., Nagler, T. and Schwaizer, G., 2016. Glacier remote sensing using Sentinel-2. Part II: Mapping glacier extents and surface facies, and comparison to Landsat 8. *Remote Sensing*, 8(7), p.575. https://doi.org/10.3390/rs8070575.

Phillips, C.L. and Nickerson, N., 2015. Soil respiration. In: *Reference Module in Earth Systems and Environmental Sciences*. Elsevier. https://doi.org/10.1016/B978-0-12-409548-9.09442-2.

Pope, A. and Rees, G., 2014. Impact of spatial, spectral, and radiometric properties of multispectral imagers on glacier surface classification. *Remote Sensing of Environment*, 141, pp.1-13. https://doi.org/10.1016/j.rse.2013.08.028

Rantanen, M., Karpechko, A., Lipponen, A. et al., 2021. The Arctic has warmed four times faster than the globe since 1980. *Preprint*, Version 1, Research Square. Available at: https://doi.org/10.21203/rs.3.rs-654081/v1 [Accessed 23 October 2024].

Ritchie, H., Rosado, P. and Roser, M., 2020. Greenhouse gas emissions. *OurWorldInData.org*. Available at: https://ourworldindata.org/greenhouse-gas-emissions [Accessed 11 October 2024]

Serrano-Silva, N., Sarria-Guzmán, Y., Dendooven, L. and Luna-Guido, M., 2014. Methanogenesis and methanotrophy in soil: A review. *Pedosphere*, 24(3), pp.291-307. https://doi.org/10.1016/S1002-0160(14)60016-3.

Thomazini, A., Mendonça, E.S., Teixeira, D.B., Almeida, I.C.C., La Scala, N., Canellas, L.P., Spokas, K.A., Milori, D.M.B.P., Turbay, C.V.G., Fernandes, R.B.A. and Schaefer, C.E.G.R., 2015. CO_2 and N_2O emissions in a soil chronosequence at a glacier retreat zone in Maritime Antarctica. *Science of The Total Environment*, 521-522, pp.336-345. https://doi.org/10.1016/j.scitotenv.2015.03.110.

Vaughan, D.G., Comiso, J.C., Allison, I., Carrasco, J., Kaser, G., Kwok, R., Mote, P., Murray, T., Paul, F., Ren, J., Rignot, E., Solomina, O., Steffen, K. and Zhang, T., 2013. Observations: Cryosphere. In: Stocker, T.F., Qin, D., Plattner, G.-K., Tignor, M., Allen, S.K., Boschung, J., Nauels, A., Xia, Y., Bex, V. and Midgley, P.M. (eds.), *Climate Change 2013: The Physical Science Basis. Contribution of Working Group I to the Fifth Assessment Report of the Intergovernmental Panel on Climate Change*. Cambridge University Press, Cambridge, United Kingdom and New York, NY, USA. pp. 317-382

Virkkala, A.-M., Niittynen, P., Kemppinen, J., Marushchak, M.E., Voigt, C., Hensgens, G., Kerttula, J., Happonen, K., Tyystjärvi, V., Biasi, C., Hultman, J., Rinne, J. and Luoto, M., 2024. High-resolution spatial patterns and drivers of terrestrial ecosystem carbon dioxide, methane, and nitrous oxide fluxes in the tundra. *Biogeosciences*, 21, pp.335–355. https://doi.org/10.5194/bg-21-335-2024.

Wang, X., Bai, X., Ma, L. et al., 2020. Snow depths' impact on soil microbial activities and carbon dioxide fluxes from a temperate wetland in Northeast China. *Scientific Reports*, 10, p.8709. https://doi.org/10.1038/s41598-020-65569-x.

Yao, Z., Zhou, H., Chen, G. and Huang, S., 2020. Dynamic changes of global fossil energy consumption structure and carbon emissions efficiency. *Advances in Climate Change Research*, 11(1), pp.9-17. https://doi.org/10.1016/j.accre.2020.03.003.

Huang, Y., Shi, W., Fu, Q., Qiu, Y., Zhao, J., Li, J., Lyu, Q., Yang, X., Xiong, J., Wang, W., Chang, R., Yao, Z., Dai, Z., Qiu, Y. and Chen, H., 2023. Soil development following glacier retreat shapes metagenomic and metabolomic functioning associated with asynchronous C and N accumulation. *Science of The Total Environment*, 892, p.164405. https://doi.org/10.1016/j.scitotenv.2023.164405

Appendix

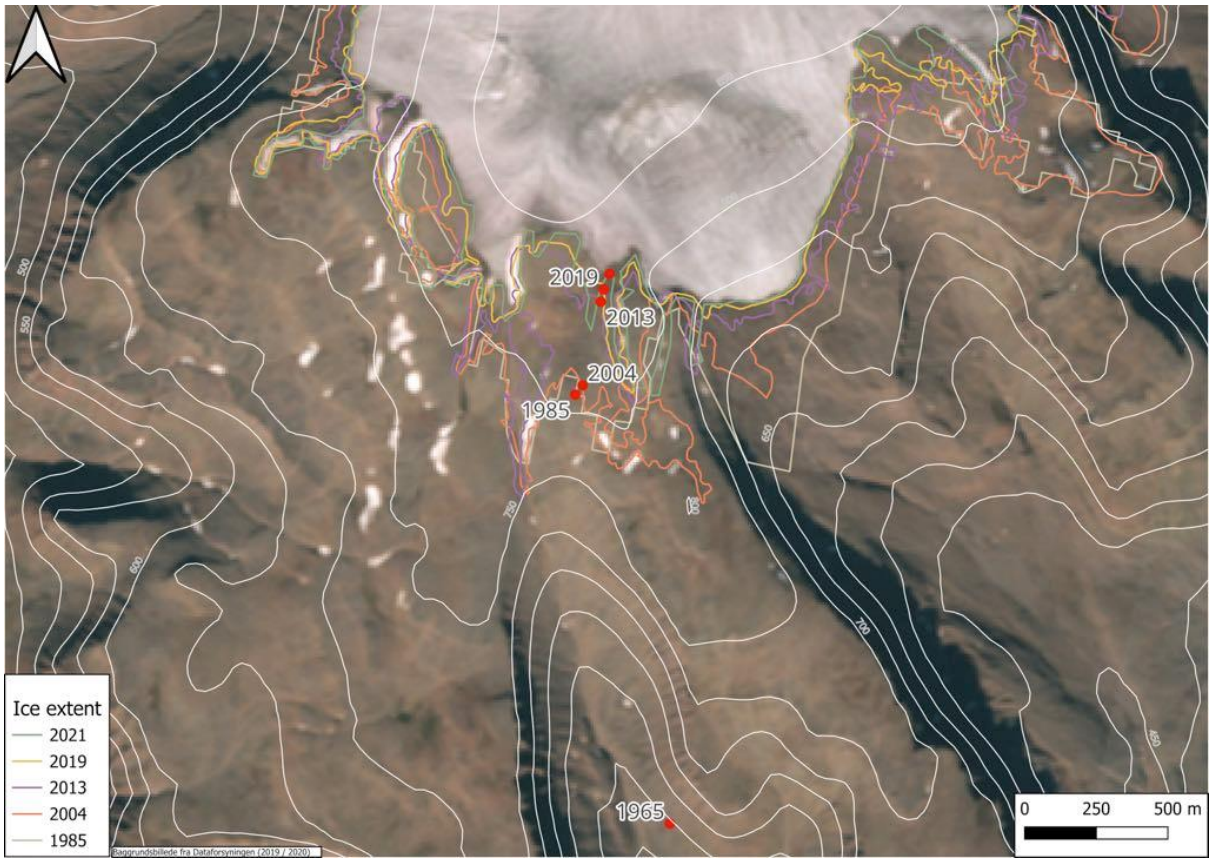

Figure A.1. The original ice extents that were used to estimate where the soil samples should be conducted.

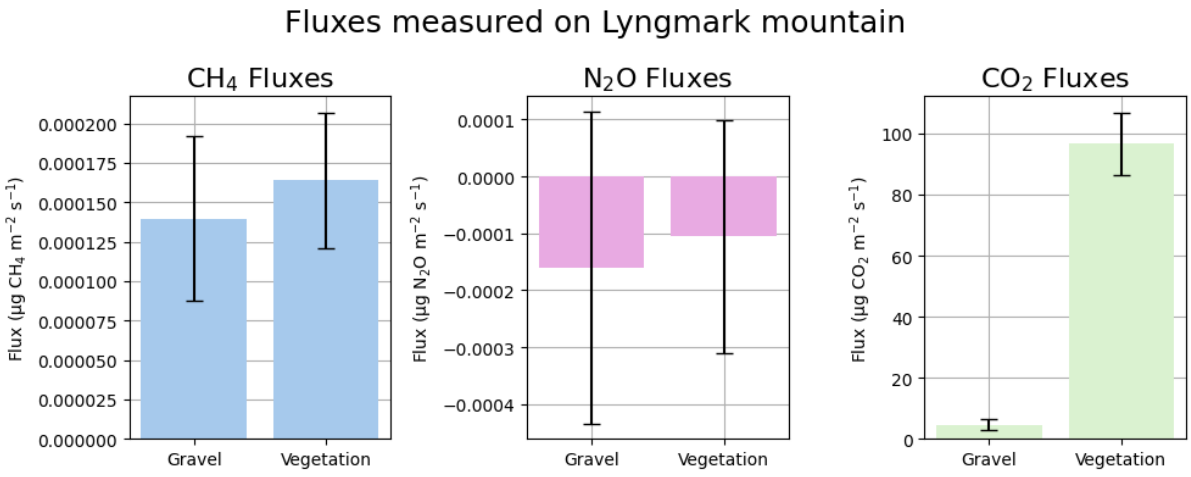

Figure A.2. In situ fluxes for gravel and vegetation.

N_2O-exchange Along the Glacial Foreland

Asta Raagaard Jønsson, Andreas Skovby Ørbæk, Freja Søeborg Lundholm

Abstract

Glacial retreat exposes expanding areas of foreland, potentially resulting in greenhouse gas exchange with the atmosphere with importance for the global climate. However, N_2O fluxes in these proglacial environments are understudied. We investigated N_2O fluxes along the glacial foreland of Lyngmarksbræen on Disko Island, Greenland. We aimed to quantify N_2O fluxes and assess whether these fluxes relate to the time since deglaciation and soil properties. We conducted both in-situ and incubation measurements of N_2O fluxes and further examined relevant soil properties. Our findings reveal both N_2O emission and uptake in the glacial foreland, with N_2O uptake being more dominant. However, the N_2O fluxes were consistently low, ranging from -7.9×10^{-4} μg m^{-2} s^{-1} (uptake) to 8.25×10^{-5} μg m^{-2} s^{-1} (emission). We show no consistent trend in N_2O flux with time since deglaciation or any significant relationship between fluxes and soil properties. The low fluxes are likely due to the minimal nitrogen content in the soil and the limited soil development in this recently deglaciated, cold environment.

Introduction

Climate change is driving the rapid decline of glaciers and ice caps worldwide, revealing increasingly larger areas of glacial foreland. As glaciers retreat and soil that was previously covered by ice is exposed, a potential for greenhouse gas exchange with the atmosphere arises. Several studies examine the CO_2 and CH4 dynamics of glacial forelands while studies of N_2O fluxes are few. Understanding N_2O dynamics in glacial forelands is crucial for accurately assessing the effects of glacial retreat on the greenhouse gas budget and thus the global climate. N_2O has an atmospheric lifetime of 120 years and a 265 times larger warming potential than CO_2 when considered over 100 years (IPCC, 2013). N_2O further causes stratospheric ozone depletion (Maag & Vinter, 1996). Although 60% of N_2O emissions originate from natural sources (IPCC, 2021), these sources are influenced by anthropogenic climate change that triggers both positive and negative feedback mechanisms that further impact the climate.

N_2O is produced by nitrification and denitrification processes carried out by microbes in the soil (Maag & Vinter, 1996). Soil nitrogen dynamics are particularly influenced by soil temperature and moisture. N_2O production increases with rising soil temperature, while the influence of soil water is more complex (Schindlbacher et al., 2004). Abundance and composition of microbes, vegetation and nitrogen content further influence N_2O fluxes.

Existing studies of N_2O on glacial forelands show little to no trend in N_2O soil production as a function of glacial retreat (Thomazini et al., 2015). According to Wei et al. (2023) this can be explained by a general low nitrogen cycling in proglacial systems. The highest N_2O production is

found at sites with the first stages of vegetation growth (Thomazini et al., 2015).

In this paper, we examine the exchange of N_2O along the glacial foreland of Lyngmarksbræen on Disko Island in Greenland. We used a chronosequence approach, where the distance from the retreating glacier serves as a proxy for time since deglaciation. We aim to address the following research questions:

1. Does the glacial foreland of Lyngmarksbræen show uptake and/or emission of N_2O?
2. How do time since deglaciation and soil properties influence N_2O exchange in the glacial foreland of Lyngmarksbræen?

Methods

Study site

The fieldwork took place in the glacial foreland of Lyngmarksbræen, located on Disko Island in Western Greenland. Lyngmarksbræen is a 20 km^2 large piece of dead ice, covering an area that has progressively diminished over the past few decades. The original plan was to collect soil samples and conduct in-situ measurements at locations previously identified at the front of the ice cap at specific times on satellite images of the glacial extent dating back to 1979. However, this plan proved unfeasible due to early snowfall this year (NSIDC, 2024), which left most of the identified locations covered by snow or ice. As a result, we adjusted our sampling strategy, selecting sites where soil was exposed while trying to follow the transect of glacial retreat. The final sampling locations are illustrated in figure 1.

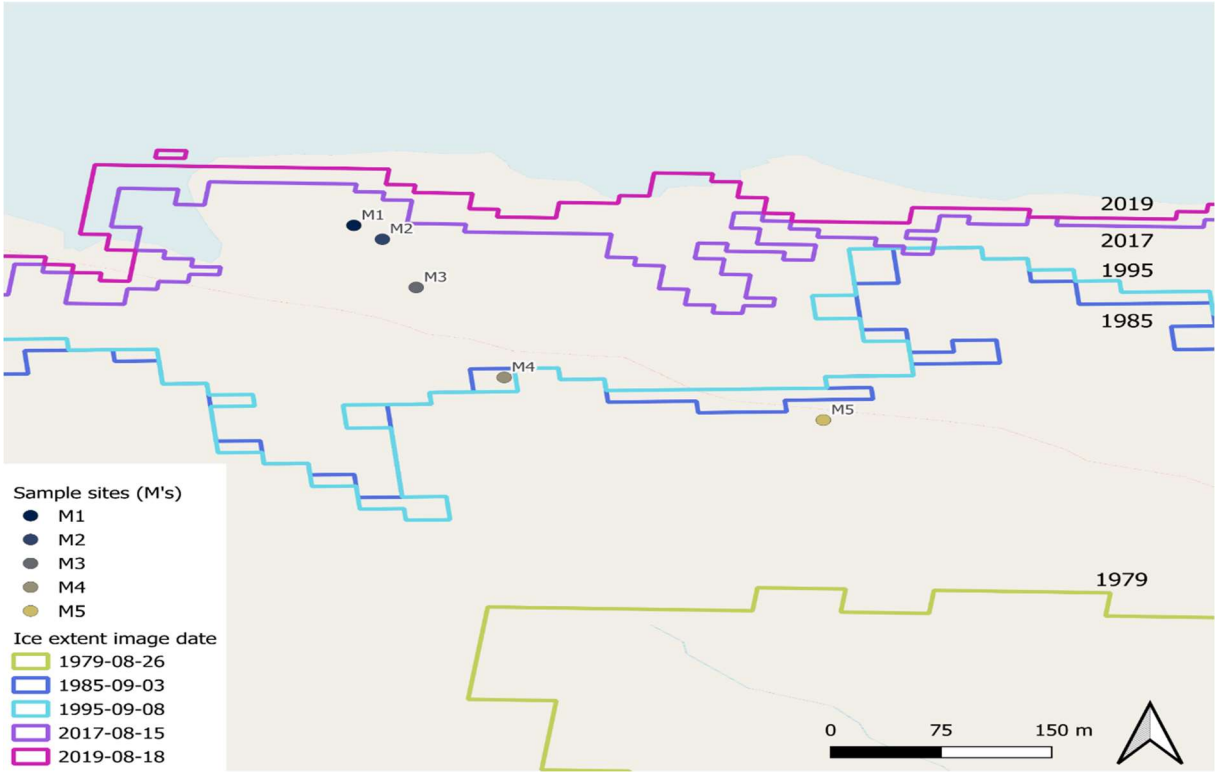

Figure 1 Specific locations for sample sites (M's) and ice extent lines for different dates.

Soil samples

A total of 42 soil samples were collected across 7 sites (M1-M7), with 3 replicates (R1-R3) and 2 depths (D1-D2). Sites M1 to M5 represent a transect from the most recently exposed soil near the glacier front to the oldest exposed soils. Due to the heterogeneous nature of the soil across the sites, sampling focused on patches resembling loam-type soil. Additionally, to assess variability, samples were taken from a more gravel-like soil (M6) and a vegetation-covered soil (M7), both located at the same site as M1 (the newest soil of the transect). The 3 replicas on each site were made to capture the natural variability at each site of the transect. The first depth (D1) was the topsoil in contact with the atmosphere, while the second depth (D2) was collected based on the soil profile. If the profile was homogenous, D2 was sampled directly beneath D1, but if a horizon change was observed, D2 was taken from the second horizon.

The soil samples were collected using steel rings with a known volume (figure 2). The ring was placed on the soil, tapped down with a hammer, and the sample was cut from the bottom with a spatula. Each sample was labeled with its site code, wrapped in parafilm to preserve moisture whilst allowing a flow of gases, and placed in open plastic bags. Upon arrival at the Arctic Station, samples were transferred to glass jars and stored in a 6 °C refrigerator for pre-incubation to standardize temperature conditions before measuring N_2O emissions or uptake

In-situ measurements

In-situ measurements of N_2O fluxes were performed using a portable N_2O gas analyzer (Licor T20) in the field. At each sampling location, where soil samples were collected, a corresponding in-situ measurement was conducted on a similar soil surface to enable direct comparison with the incubation results. For site M1, three replicate measurements were taken on loamy soil, three on gravel, and three on vegetation. For the rest of the transect, three replicate measurements were performed on loamy surfaces, representing the same soil type as the soil samples. Each measurement lasted 8-12 minutes to ensure sufficient data was captured to stabilize and accurately record the gas flux. Unfortunately, the gas analyzer malfunctioned at site M3 due to precipitation entering the device, preventing measurements from being completed on the remaining transect sites (M4-M5).

Since this was the first time N_2O measurements were conducted at Lyngmarksbræen, we installed permanent plastic frames at each site to facilitate future measurements (figure 3). During the measurement process, a chamber with a known volume was placed on these frames. The chamber had two tubes attached to the inlet and outlet, creating a closed system that allowed the analyzer to measure gas emissions or uptake. Inside the chamber, a turbine simulated atmospheric turbulence, ensuring even gas mixing. Simultaneously, air temperature inside the chamber was recorded with a thermometer, together with soil moisture and soil temperature.

Figure 2 Taking soil samples using steel rings.

Soil incubations

The laboratory incubations of the soil samples were carried out using the same machine and method as for the in-situ measurements, except the gas analyzer tubes were connected to a glass jar with an airtight-lid and the gas analyzer was run for 4 minutes. The 4-minute measurement time was the standard time Claudia Fiencke (Universität Hamburg, n.d.) used when incubating. After incubation, the soil sample was weighed, sorted for stones and vegetation, and put in plastic bags for transportation. A 10 g sub-sample was brought back home for further soil components analysis back in Copenhagen.

Soil properties analysis

For each sample, the pH was measured, and the water content was calculated from the difference in weight from a 5 g sample after drying at 105 °C for 22 hours. The oven dried soil was homogenized by ball-mining, and a 30-40 mg subsample was weighed into tin combustion cups for measurement of the total carbon (TC) and total nitrogen (TN) (Wang et al., 2019).

Calculating N_2O flux

The flux of N_2O was calculated using a MATLAB script developed by Kutzbach et al. (2007). The fluxes have been calculated for the 14 in-situ measurements, as well as the 44 soil samples, which were analyzed in the lab. For each three replicas, a mean was found as well as a standard deviation.

The MATLAB script allowed visual inspection of each sampling to determine start and end points of the measurement to use for calculation of the flux. An example of this can be seen in appendix 1.

From the visual inspections a standard discard of the first and last 10

Figure 3 In-situ measurements

seconds of the measuring intervals was applied, which means that the first and last 10 seconds were not included in the calculations of the flux.

Minimum detectable flux (MDF)

For all the measurements, the minimum detectable flux (MDF) could be calculated according to the method by Christensen et al. (2015). Here it is calculated as:

$$MDF = \left(\frac{A_A}{t_c \sqrt{\frac{t_c}{p_s}}} \right) \left(\frac{VP}{SRT} \right)$$

Here A_A is the instrument precision, t_c is the measured time, p_s is the sampling periodicity, V is chamber volume, P is atmospheric pressure, S is surface area, R is the gas constant and T is the temperature. All of these were assumed to be constant for each method, in-situ measurements and laboratory measurements respectively, as the chamber size and the sampling period length are the only variables.

The MDF was for lab measurements at 4 minutes calculated to be 4.76×10^{-6} µg m^{-2} s^{-1} and for in-situ measurements at about 12 minutes it was calculated to be 8.94×10^{-6} µg m^{-2} s^{-1}.

Results

Incubation result

The incubation results show very small N_2O uptake rates for most of the soil samples with mean values across replicates ranging between -3.71×10^{-5} and -2.54×10^{-4} µg m^{-2} s^{-1} (figure 4). Contrarily, two of the samples (M4D2 and M6D1) shows N_2O emissions of 8.02×10^{-5} and 8.25×10^{-5} µg m^{-2} s^{-1}, respectively. Notably, the highest values for both uptake and emission are observed within the same soil profile at the gravel site (M6), where the topsoil emits N_2O, while the second depth layer shows N_2O uptake. The vegetation samples (M7) show consistent N_2O uptake.

Soil samples M1 to M5 represent the transect from the most recently exposed to the oldest exposed soils. In the topsoil samples (D1) along this transect, there is a visible trend of decreasing N_2O uptake with increasing time since deglaciation (figure 5). However, this trend is not statistically significant, with an R^2 value of 0.616. In contrast, N_2O fluxes from the second depth layer (D2) show no trend in relation to time since exposure (figure 5).

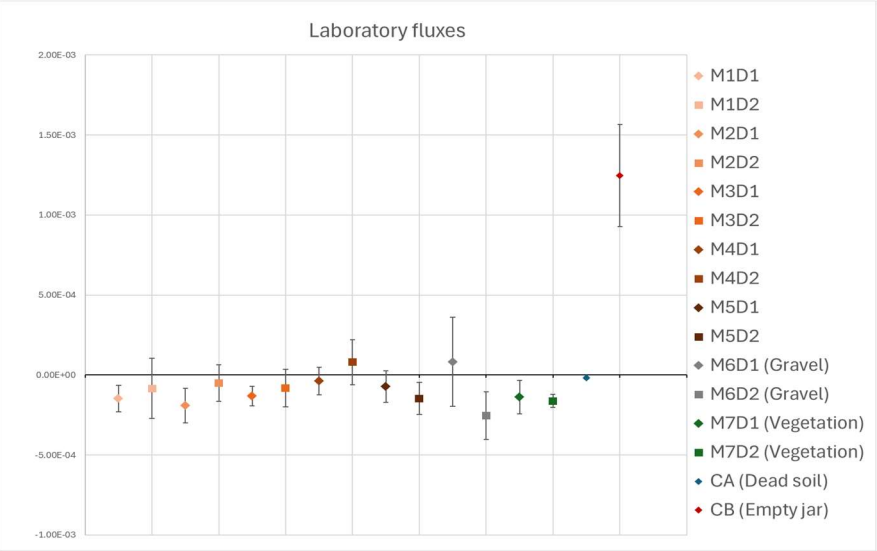

Figure 4: Laboratory N_2O fluxes - incubation results for each soil sample depth. Each point represents a soil sample (mean value of replicas). Error bars show the variation between replicas.

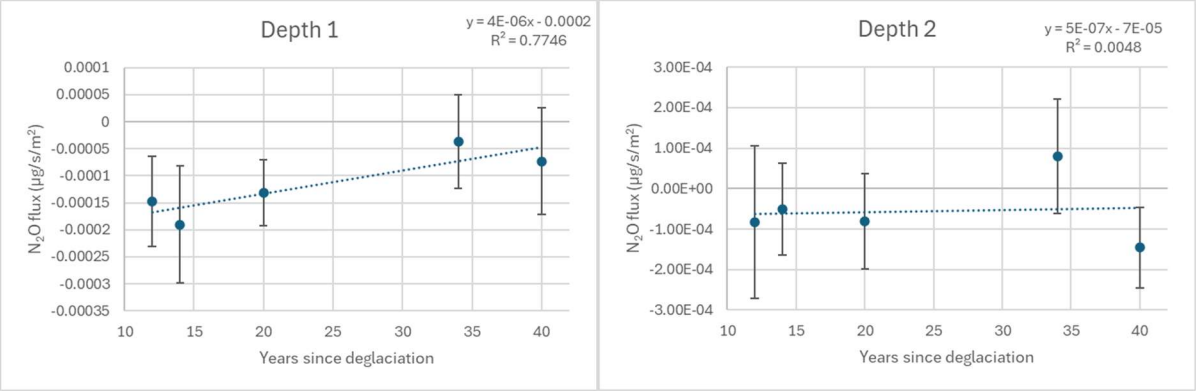

Figure 5: N_2O fluxes for transect M1-M5 plotted against time since deglaciation for depth 1 and 2 respectively. Each point represents a soil sample (mean value of replicas). Error bars show the variation between replicas.

Replicate variation of the soil samples is generally high. In 7 out of 14 samples, the mean flux exceeded the standard deviation of the replicates, all of which were associated with N_2O uptake, suggesting a robust although small signal from these soils. In contrast, for the two samples showing N_2O emissions, the standard deviation between replicates was larger than the flux means.

The empty-jar standard shows a much larger flux than the soil samples of 1.247×10^{-3} µg m^{-2} s^{-1}, accompanied by significant variation between replicates. This standard was excluded from analysis. Instead, the dead-soil standard, which shows flux values close to zero and no detectable variation between replicates, was used as a reliable control. As the MDF for laboratory flux measurements of 4 minutes was calculated as 4.76×10^{-6} µg m^{-2} s^{-1}, all the sampled fluxes were larger than the MDF.

In-situ results

The in-situ N_2O flux measurements generally indicate a small uptake of N_2O, with mean uptake values across replicates ranging from -1.1×10^{-4} to -7.9×10^{-4} µg m^{-2} s^{-1} (Figure 6), with the highest uptake observed at site M3. In contrast, site M1 exhibited a mean N_2O emission of 3.22×10^{-5} µg m^{-2} s^{-1}. The gravel and vegetation site (M6 and M7) both show uptake as a means of replicates, however for sites M1, M6, and M7, the standard deviation of replicates exceeded the mean flux, leaving only M2 and M3 with consistent signals across replicates.

Along the transect from M1 to M3, there is a linear increase in N_2O uptake, suggesting an upward trend in uptake with increasing time since deglaciation. However, this trend lacks statistical significance, as the model is based on only three data points and has an R^2 value of 0.98 (Figure 7).

As the MDF for in-situ flux measurements of 12 minutes was calculated as 8.94×10^{-6} µg m^{-2} s^{-1}, all the sampled fluxes were larger than the MDF.

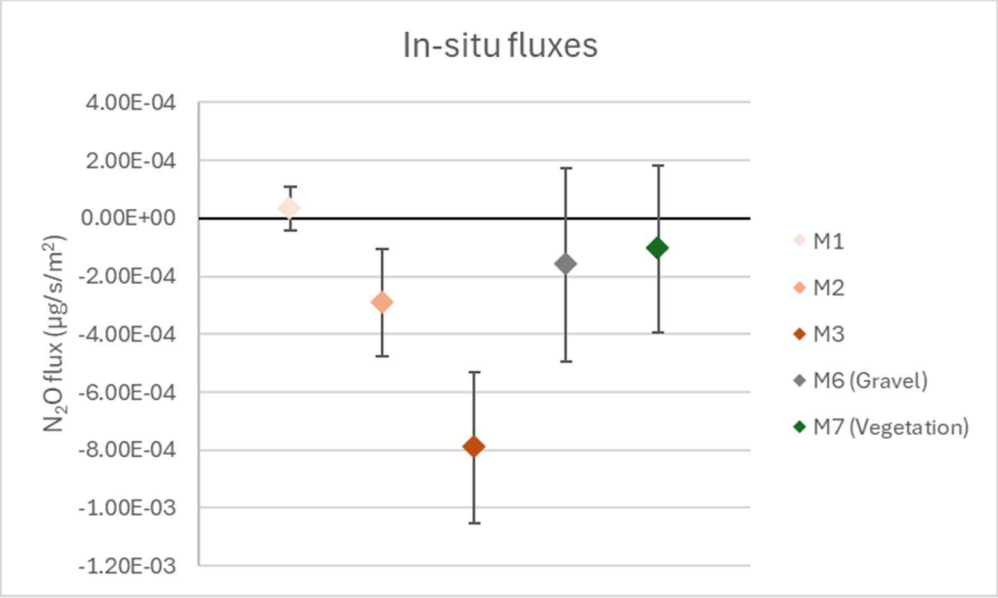

Figure 6: Transect (M1-M3) and M6 and M7 samples taken at M1 site, each point represents a soil sample (mean value of replicas). Error bars show the variation between replicas.

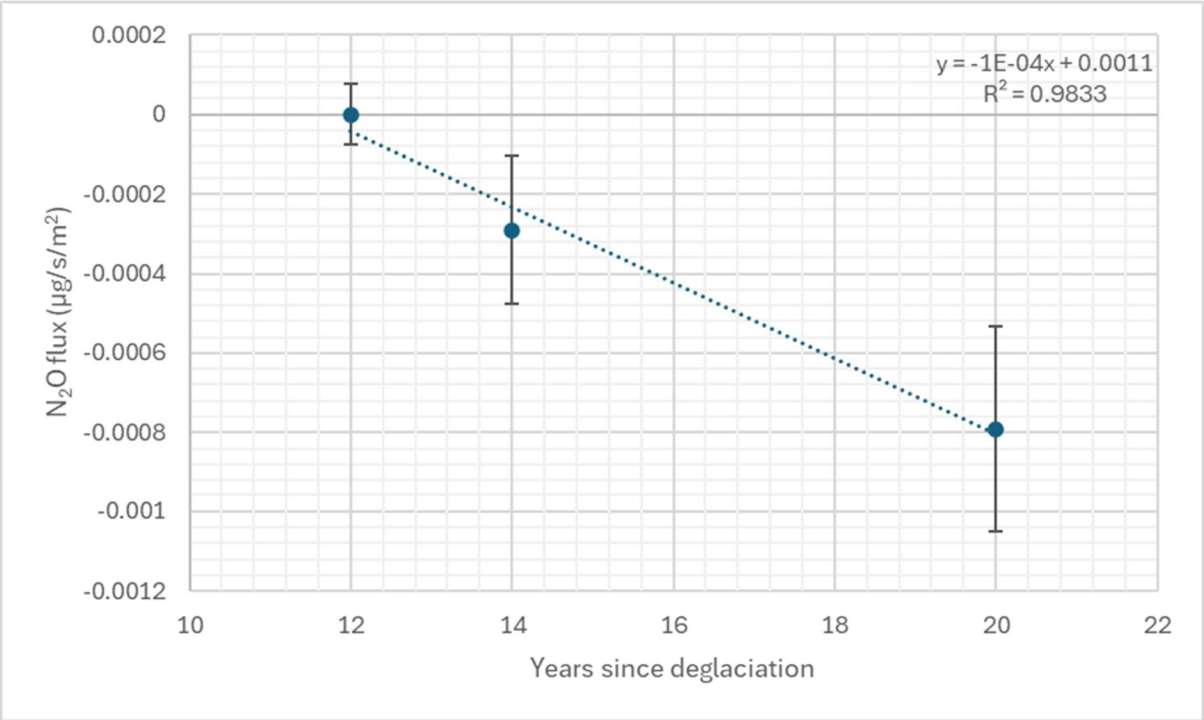

Figure 7: Transect section (M1-M3) the trend expressed in a linear regression. Each point represents a soil sample (mean value of replicas). Error bars show the variation between replicas.

Soil properties results

The soil samples are predominantly neutral, with pH values ranging from 5.85 to 7.86. Samples M1 to M4 consistently exhibit neutral pH values between 7.0 and 7.86, while M5, M6, and M7 are more acidic, with the vegetation site (M7) having the lowest pH. Soil water content varies widely, ranging from 1.73% to 56.88% from the driest to the wettest sample.

Both nitrogen and carbon contents are consistently low across all samples. TN ranges from 0.009% to 0.0272%, and TC ranges from 0.062% to 0.307%. While

nitrogen content shows little variation between sites, carbon content is higher at site M7 with vegetation growth. The C/N ratio is low across all samples, with values between 4.94 and 13.82, reflecting low carbon levels relative to nitrogen despite both being present in small amounts. The results for soil properties are presented in appendix 2.

Discussion

N2O flux results

The glacial foreland of Lyngmarksbræen shows both uptake and emission of N_2O in both our incubation and in-situ results. However, the fluxes are consistently small in magnitude, with the highest mean flux being an N_2O uptake of -7.9×10^{-4} μg m^{-2} s^{-1}, measured in-situ. Both incubation and in-situ measurements show N_2O uptake in most samples and emission in only a few. Notably, the N_2O uptake is significantly larger in the in-situ measurements, approximately 21 times greater than in the incubations, while the N_2O emissions are of a similar magnitude between both methods.

Although the fluxes are small, they are all above the calculated detection limits for each method, making them reliable signals. However, both methods show considerable variability between replicates. Half of the incubation samples and three-fifths of the in-situ measurements exhibit variation between replicates that exceeds the mean flux, indicating inconsistent results. In the field, replicates were taken from the same patch of soil, but the site's heterogeneity made it nearly impossible to sample identical spots. The variability observed in the replicates reflects the natural heterogeneity of the site, which was already visually apparent during fieldwork.

Differences in flux results

There are clear differences between our incubation and in-situ results, not only in their magnitudes but also in their directions. While M1 shows N_2O uptake in the incubation results, it exhibits emission in the in-situ measurements. However, the remaining in-situ results align with the general trend observed in the incubation data.

In addition to methodological variations, the differences in results between methods can be explained by the challenge in finding homogeneous soil profiles for in-situ measurements and soil samples for incubation. Because the plastic tubes for in-situ measurements were permanently installed, soil samples were collected from nearby but distinct patches.

Additionally, the incubation results represent two distinct soil depths for each site, whereas the in-situ measurements encompass the entire soil profile. As a result, we should not expect completely comparable outcomes, which is further highlighted by the contrasting flux directions observed at some sites. Notably, the highest values for both uptake and emission in the incubation results occur at the gravel site (M6) for the two different depths.

Time since deglaciation

Analyzing the transect that represents time since deglaciation reveals differing N_2O flux results for time since exposure for the two methods. The incubation results for topsoil samples (M1-M5) indicate a trend of decreasing N_2O uptake with increasing time since deglaciation. In contrast, the in-situ measurements show a linear increase in N_2O uptake with increasing time since exposure. However, the trend in incubation

results is not statistically significant, and the in-situ measurements have too few data points to be considered reliable. Additionally, the incubation results for the second soil depth along the transect (M1-M5) show no trend related to time since deglaciation. The opposing and in-significant trends suggest that there is no consistent relationship between N_2O fluxes and time since deglaciation.

Our findings related to fluxes and time since deglaciation are influenced by uncertainties regarding sample transect, as well as insufficient data on the dating of the glacial extent. A primary difficulty was tracking the deglacial lines presented in figure 1. The weather conditions, snow, ice, and steep topography made it impossible to collect samples and measurements at our initial targeted locations. Additionally, the Licore gas analyzer malfunctioned due to high humidity, preventing in-situ measurements at M4-M5. These challenges are inherent to field research, especially in Greenland, where adapting to the terrain and rapidly changing weather is crucial.

Our restricted mobility in the glacial foreland meant we could not sample areas that we consider having deglaciated after 2017 or before 1971 (figure 1). Samples M1-M3 are considered to have deglaciated between 1995 and 2017, but without glacial retreat lines within this period, we cannot be sure that the M1-M3 transect accurately represents time since deglaciation, leaving the in-situ results on this matter unreliable.

Despite methodological challenges, our results are in line with similar studies in Antarctica. Wang et al. (2020) examined the combined effects of glacial retreat and penguin activity on soil greenhouse gas fluxes on South Georgia in sub-Antarctica and found that N_2O production was not influenced by exposure time. Similarly, Thomazini et al. (2015) examined CO_2 and N_2O emissions in a soil chronosequence at a glacier retreat zone in Maritime Antarctica and found no trend in soil N_2O.

Influence of soil properties

Our results show no consistent differences in N_2O fluxes among the loamy, gravel, and vegetation soil samples collected from the same site (M1, M6, and M7), as all generally show low rates of N_2O uptake. The gravel samples are particularly noteworthy since incubation results reveal N_2O emission in the topsoil and uptake in the second depth, while in-situ measurements show an overall uptake as the mean of replicates, although one replicate showed emission. The vegetation samples consistently demonstrate N_2O uptake, with only one replicate exception in the in-situ measurements. This finding contrasts with Thomazini et al. (2015), who observed that maximum N_2O production occurred at sites undergoing the initial stages of vegetation growth in a glacier retreat zone in Maritime Antarctica.

The consistently low TN content in the soil samples suggests a limited potential for N_2O emission and production, as nitrifying and denitrifying bacteria have insufficient substrate (ammonium or nitrate) to convert into N_2O. However, we do not know the specific forms of nitrogen present in the soil. There is no clear relationship between TN and N_2O fluxes across the samples, but the variation in TN among the samples is also minimal. The low TC content across the soil samples indicates limited soil development and microbial activity. While variations in TC are more pronounced than for TN there is still no apparent relationship with N_2O fluxes. Additionally, the low C/N ratios of

the soil samples suggest relatively good nitrogen availability for microbial processes that could drive N_2O fluxes, which might indicate a lack of microbial presence in the soil.

The pH values of the soil samples do not show any relationship with the N2O fluxes either. This was not expected either since all of the samples are near-neutral and the pH-values should therefore not be limiting for microbial activity (Skiba, 2008). The same can be said for the water content.

Overall, the low nitrogen content, coupled with minimal soil development and microbial activity, appears to be the most plausible explanation for the very low N_2O fluxes observed in the glacial foreland of Lyngmarksbræen. This observation aligns with the site's low temperatures and relatively recent deglaciation. Soil development at these latitudes occurs over extended timescales, as soil processes are constrained by low temperatures, short growing seasons, and slow weathering rates (Turpin-Jelfs et al., 2019). In a study examining nitrogen cycling in microbial communities within a glacier forefield in Switzerland, Brankatschk et al. (2010) found that significant N_2O uptake and emission processes began after 50–70 years and 120–200 years, respectively.

Conclusion

The N_2O fluxes in the glacial foreland of Lyngmarksbræen on Disko Island, Greenland, reveals both N_2O uptake and emissions although at consistently low flux levels. The measured N_2O fluxes ranged from -7.9 × 10^{-}4 μg m^{-2} s^{-1} (uptake) to 8.25 × 10^{-5} μg m^{-2} s^{-1} (emission). Notably, in-situ measurements indicated significantly higher N_2O uptake compared to emissions, which were similar in magnitude across both incubation and in-situ measurements. No consistent trends in N_2O flux were observed in relation to time since deglaciation, with opposing relationships emerging from the two measurement methods, neither of which were statistically significant. Additionally, no clear relationships were found between N_2O fluxes and various soil properties such as pH, C/N ratio, and water content, however, the TN content of the soils were consistently very low. The low N_2O fluxes can be attributed to the low TN content in the soil, coupled with minimal soil development due to low temperatures and the recent nature of deglaciation in this area.

References

Brankatschk, R., Töwe, S., Kleineidam, K., Schloter, M., & Zeyer, J. (2011). Abundances and potential activities of nitrogen cycling microbial communities along a chronosequence of a glacier forefield. The ISME Journal, 5(6), 1025–1037. https://doi.org/10.1038/ismej.2010.184

Christiansen, J., Outhwaite, J., & Smukler, S. (2015). Comparison of CO_2, CH_4 and N_2O soil-atmosphere exchange measured in static chambers with cavity ring-down spectroscopy and gas chromatography. Agricultural and Forest Meteorology, 211, 48–57. https://doi.org/10.1016/j.agrformet.2015.06.004

IPCC. (2013). Climate Change 2013: The Physical Science Basis. Contribution of Working Group I to the Fifth Assessment Report of the Intergovernmental Panel on Climate Change. Cambridge University Press, Cambridge, United Kingdom and New York, NY, USA, 1535 pp.

IPCC. (2021). Climate Change 2021: The Physical Science Basis. Contribution of Working Group I to the Sixth Assessment Report of the Intergovernmental Panel on Climate Change. Cambridge University Press, Cambridge, United Kingdom and New York, NY, USA, 2391 pp.

Kutzbach, L., Schneider, J., Sachs, T., Giebels, M., Nykänen, H., Shurpali, N. J., Martikainen, P. J., Alm, J., & Wilmking, M. (2007). CO_2 flux determination by closed-chamber methods can be seriously biased by inappropriate application of linear regression. Biogeosciences, 4, 1005–1025. https://doi.org/10.5194/bg-4-1005-2007

Maag, M., & Vinther, F. P. (1996). Nitrous oxide emission by nitrification and denitrification in different soil types and at different soil moisture contents and temperatures. Applied Soil Ecology, 4(1), 5–14. https://doi.org/10.1016/0929-1393(96)00106-0

NSIDC. (2024). No medal for Greenland melt in 2024. National Snow and Ice Data Center, CIRES at the University of Colorado Boulder. Retrieved September 24, 2024, from https://nsidc.org/ice-sheets-today/analyses/no-medal-greenland-melt-2024

Schindlbacher, A., Zechmeister-Boltenstern, S., & Butterbach-Bahl, K. (2004). Effects of soil moisture and temperature on NO, NO_2, and N_2O emissions from European forest soils. Journal of Geophysical Research: Atmospheres, 109(D17). https://doi.org/10.1029/2004JD004590

Skiba, U. (2008). Denitrification. In Earth Systems and Environmental Sciences (pp. 866–871). ScienceDirect.

Thomazini, A., Mendonça, E. S., Teixeira, D. B., Almeida, I. C. C., La Scala, N., Canellas, L. P., Spokas, K. A., Milori, D. M. B. P., Turbay, C. V. G., Fernandes, R. B. A., & Schaefer, C. E. G. R. (2015). CO_2 and N_2O emissions in a soil chronosequence at a glacier retreat zone in Maritime Antarctica. Science of The Total Environment, 521–522, 336–345. https://doi.org/10.1016/j.scitotenv.2015.03.110

Turpin-Jelfs, T., Michaelides, K., Blacker, J. J., Benning, L. G., Williams, J. M., & Anesio, A. M. (2018). Distribution of soil nitrogen and nitrogenase activity in the forefield of a High Arctic receding glacier. Annals of Glaciology. https://doi.org/10.1017/aog.2018.35

Universität Hamburg. (2024). Dr. Claudia Fiencke, Institute of Soil Science. Retrieved October 14, 2024, from https://www.geo.uni-hamburg.de/en/bodenkunde/personen/claudia-fiencke.html

Wang, P., D'Imperio, L., Biersma, E. M., Ranniku, R., Xu, W., Tian, Q., Ambus, P., & Elberling, B. (2020). Combined effects of glacial retreat and penguin activity on soil greenhouse gas fluxes on South Georgia, sub-Antarctica. Science of The Total Environment, 718, 135255. https://doi.org/10.1016/j.scitotenv.2019.135255

Wei, J., Fontaine, L., Valiente, N., Dörsch, P., Hessen, D. O., & Eiler, A. (2023). Trajectories of freshwater microbial genomics and greenhouse gas saturation upon glacial retreat. Nature Communications, 14, 3234. https://doi.org/10.1038/s41467-023-38806-w

Appendix

Appendix 1: Visual inspection of flux

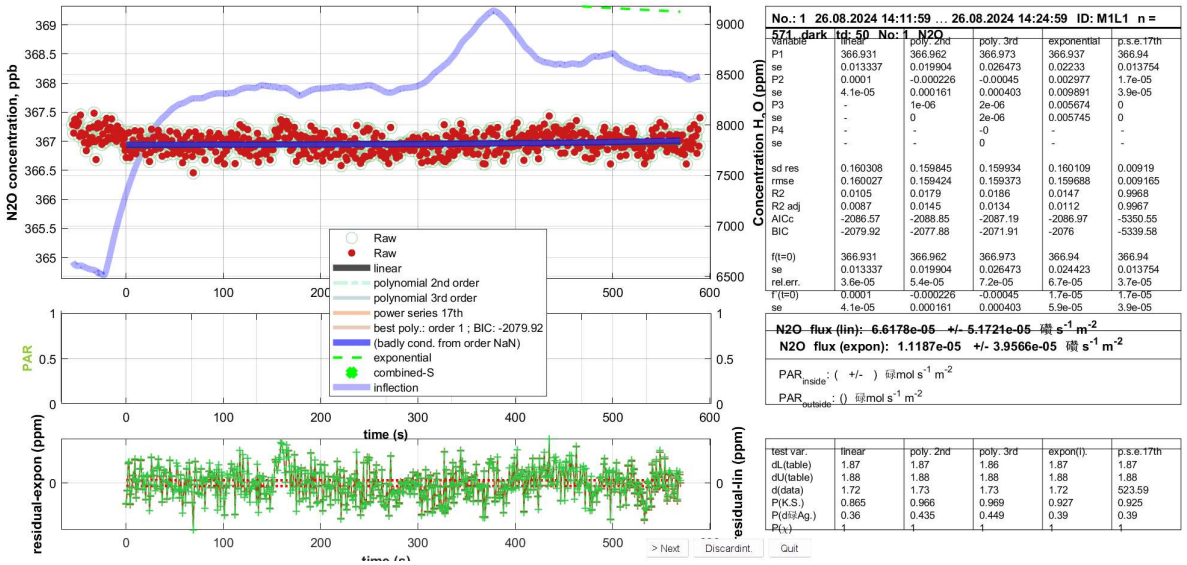

variable	linear	poly. 2nd	poly. 3rd	exponential	p.s.e.17th
P1	366.931	366.962	366.973	366.937	366.94
se	0.013337	0.019904	0.026473	0.02233	0.013754
P2	0.0001	-0.000226	-0.00045	0.002977	1.7e-05
se	4.1e-05	0.000161	0.000403	0.009891	3.9e-05
P3	-	1e-06	2e-06	0.005674	0
se	-	0	2e-06	0.005745	0
P4	-	-	-0	-	-
se	-	-	0	-	-
sd res	0.160308	0.159845	0.159934	0.160109	0.00919
rmse	0.160027	0.159424	0.159373	0.159688	0.009165
R2	0.0105	0.0179	0.0186	0.0147	0.9968
R2 adj	0.0087	0.0145	0.0134	0.0112	0.9967
AICc	-2086.57	-2088.85	-2087.19	-2086.97	-5350.55
BIC	-2079.92	-2077.88	-2071.91	-2076	-5339.58
f(t=0)	366.931	366.962	366.973	366.94	366.94
se	0.013337	0.019904	0.026473	0.024423	0.013754
rel.err.	3.6e-05	5.4e-05	7.2e-05	6.7e-05	3.7e-05
f'(t=0)	0.0001	-0.000226	-0.00045	1.7e-05	1.7e-05
se	4.1e-05	0.000161	0.000403	5.9e-05	3.9e-05

test var.	linear	poly. 2nd	poly. 3rd	expon(t).	p.s.e.17th
dL(table)	1.87	1.87	1.86	1.87	1.87
dU(table)	1.88	1.88	1.88	1.88	1.88
d(data)	1.72	1.73	1.73	1.72	523.59
P(K.S.)	0.865	0.966	0.969	0.927	0.925
P(d≥Ag.)	0.36	0.435	0.449	0.39	0.39
P(x)	1	1	1	1	1

Figure A1. The inspection of a single sampling through the MATLAB script by Kutzbach et al. (2007)

Appendix 2: Soil properties results

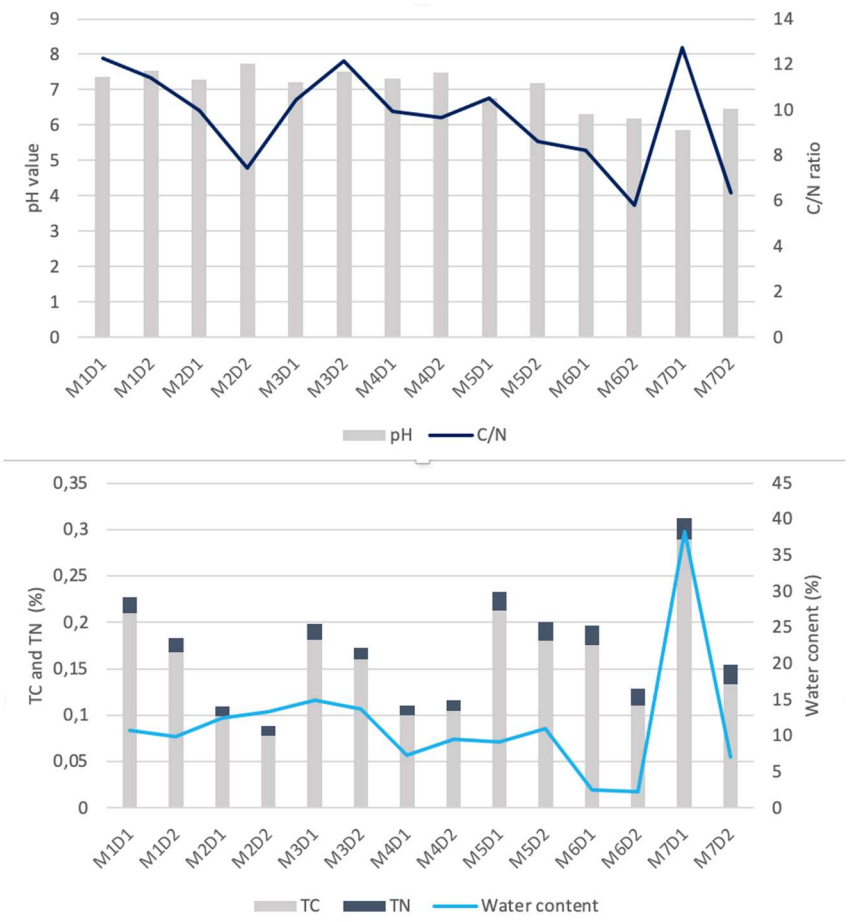

Figure A2: Soil properties results from laboratory analysis for pH, water content, total carbon (TC), total nitrogen (TN) and C/N-ratio.

Methane fluxes along a transect in Blæsedalen

Karla Marie Jokumsen Nielsen, Sara Liv Christiansen Thrane & Dian Liu

Abstract: This study examines the dynamics between methane (CH_4) fluxes, vegetation and soil properties along a transect in Blæsedalen on Disko Island in West Greenland. The fieldwork was carried out at the end of August during which soil samples, vegetation detection and in situ measurement were done. In the laboratory, CH_4 incubation measurements, pH-test and an elementary analysis were carried out. In general, dry heath in the uppermost part of the transect (P1) had the highest uptake of CH_4, dry heath further down the transect (P2) had a net uptake, but less than P1, the fen area furthest down the transect (P3) showed a net release, and the hummock (H) has net uptake. The in situ measurements revealed correlations between soil moisture and temperature, with higher soil moisture and lower temperature leading to increased CH_4. The incubation did not show any correlation with any soil or vegetation properties. However, similar trends were seen with regards to soil moisture; P3 had higher soil moisture than the other points. Furthermore, a higher % C was estimated in P3 and H in the topsoil, which were the ones with most plant roots, and P1 as well as P2 were similar in % C. Furthermore, the study calculates a rough estimate of the area-integrated CH_4-budget of Blæsedalen in the growing season, and finds that Blæsedalen is a net sink of - 3,77 kg CH_4-C.

Introduction

The global average temperature is rising, especially in the Arctic, in which post-industrial warming is expected to reach approximately 4-6°C by the end of the 21st century (D'Imperio et al., 2016). Consequently, this has emphasized the need to understand how the natural sinks and sources of methane (CH_4) will respond to temperature changes. CH_4 is a potent greenhouse gas with a global warming potential 28 times greater than that of carbon dioxide (CO_2), when measured on a mass basis over a 100-year time frame. The warming of the Arctic could influence substrate availability, organic matter decomposition, plant growth, and plant species composition, potentially altering the exchange of CH_4 between the soil and the atmosphere (Nielsen et al., 2017). At present, the Arctic is regarded as a net source of (15–50 Tg CH_4 per year), with the largest biogenic emissions coming from water-saturated, carbon-rich soils (D'Imperio et al., 2023). However, Greenland is considered a net sink, having an uptake of 65.000 tons methane from dry soils, while wetlands release 9.000 tons during the year (Elberling et al., 2024). Therefore, the aim of this study is to examine the CH_4 fluxes along a transect that spans from dry to wet, and which is covered by different vegetation (dry heath and fen) in order to see how CH_4 fluxes variate. Furthermore, it is wished to determine whether the transect is a net source or sink of CH_4 when scaled up to the entire research area. As part of this research, different soil

properties and vegetation types will be examined. The research has been carried out in Blæsedalen on Disko Island in Greenland.

Theory

Soil moisture and temperature

Methane production and oxidation depends on several abiotic and biotic factors (D'Imperio et al., 2016). Among the abiotic factors regulating CH_4 dynamics, soil moisture and temperature are considered as main drivers (Elberling et al., 2024; D'Imperio et al., 2016). Warmer temperature enhances microbial activity, which increases the rate of methan production and oxidation. In an anaerobic environment, microorganisms (methanogens) use CO_2, H_2 and chemical compounds, formate and acetate, as substrates to produce methane (Nielsen et al., 2017). Methane release occurs in two ways; either through the soil or through plant roots. In Blæsedalen, the dominating grass type *Carex* have developed large, air-filled roots, aerenchyma, which transport oxygen down to the water saturated part of the soil. However, this also enables CH_4 to diffuse through the roots to the atmosphere (Nielsen et al., 2017). In soils with oxygen availability, two types of microorganisms oxidize CH_4 into CO_2. Low affinity microorganisms use a small amount of oxygen from the top soil, oxidizing high concentrations of CH_4 in wet soils, and reducing CH_4 release in wetlands. High affinity microorganisms oxidize small amounts of CH_4 directly from the atmosphere in dry soils (Elberling et al., 2024).

Vegetation

Vegetation is another key factor regulating CH_4 fluxes in soils. In Greenland, CH_4 uptake is observed in dry heath tundra and areas without vegetation, while CH_4 release occurs in wetlands and moist, vegetated areas. In Blæsedalen, the dry heath vegetation consists of deciduous dwarf shrubs such as *Betula nana*, *Vaccinium uliginosum*, and *Salix glauca*, as well as evergreen low shrubs like *Cassiope tetragona* and *Empetrum nigrum*. Fens are characterized by vegetation dominated by sedges, mosses, and *Salix arctophila* (D'Imperio et al., 2016).

C:N ratio and % C

Furthermore, the C:N ratio, which is controlled by the specific plant types present in the soil, is also a key factor in regulating both CH_4 oxidation and production. A low C:N ratio indicates a surplus of organic N available for plant growth, which increases C turnover in soil (Elberling, 2020). With regards to C content, a higher amount is expected in wetlands, compared to upland soils, due to a slower decomposition rate (Christiansen et al. 2014; D'Imperio et al. 2016).

Hummock

The hummocks (H) are elevated areas, with hollow areas in between. In the Arctic, they are created by cryogenic environments in permafrost or wetland ecosystems, including the Arctic tundra, where they play a significant role in soil processes and gas exchange (Ruiz-Fernández et al., 2020). The hummocks are relatively dry compared to the hollow parts, and therefore contain both types of CH_4 oxidizing microorganisms, in contrast to the hollow parts, which only host low-affinity microorganisms. The hummocks therefore have favourable conditions for

methane oxidation. Furthermore, hummocks are typically rich in vascular plant communities (Sullivan et al., 2007).

Methods

Description of study area

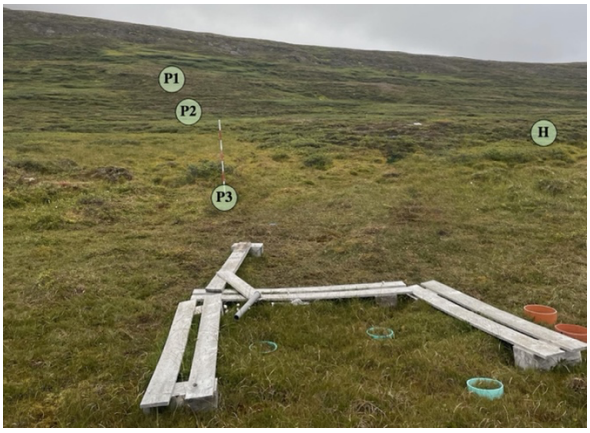

Figure 1: Picture with marks of the four sampling points.

The field work was carried out along a transect of 218 meters in Blæsedalen on Disko Island in West Greenland, which is located at 69°26'N, -53°46'W. Blæsedalen is a valley containing different vegetation and soil characteristics, and the growing season occurs from June to late September (D'Imperio et al., 2016). Soil samples, in situ measurements and vegetation detections were conducted at the end of August in 2024. The fieldwork was carried out at four points along the transect (Figure 1). Point 1 (P1) was the highest located point and Point 3 (P3) was the lowest. The research also included hummocks, which is located next to the transect, between P2 and P3.

In situ measurements

In situ measurements were conducted with LI-COR gas analyzer during a three-minute period. Measurements of CH_4, CO_2 and H_2O were carried out on top of three column rings within each point, P1, P2, P3 and H, which corresponded to the specific vegetation characteristics of each area. A closed chamber with a fan was used to circulate air inside the chamber, ensuring uniform gas concentration. The gas concentration was subsequently multiplied by the volume of the chamber, which depended on a specific column height for each measurement. The volume ranged between 0.00937491 m^3 and 0.01114205 m^3.

Soil sampling

A total of 33 soil samples were collected in the field, consisting of three replicates from each sampling point. The three replicates were taken in areas that had the same vegetation cover as the locations where in situ measurements were conducted. For each replicate, one soil sample was taken from each layer, resulting in three depths for all replicates in plot P1, P2, and P3. The hummock only had two distinct layers, therefore only two soil samples were taken from each replicate. In addition, the soil samples were only assembled from the top of the hummock, and not from the hollow parts. For P1 and P2, the soil samples were collected using a retention ring, with a height of 3.5 cm and a volume of 100cm^3, at each depth, while at P3 and the hummock, the samples were cut into squares, due to the presence of roots, and then placed into retention rings. The samples were taken from the top of each layer downward, after characterizing and measuring the depth of each layer. All samples were wrapped in parafilm to preserve the natural soil conditions. Each sample was placed into a

plastic bag with air holes, further wrapped in a paper bag, and transported to the laboratory.

Plant species detection

Additionally, plant species were detected in each of the three replicates within each plot using the Quadrat Method. The quadrat was positioned to match the vegetation cover at the locations where soil samples were collected, and plant type and the height of the central plant was defined and measured diagonally (total of 18 squares).

Laboratory work on Disko

In the laboratory, each soil sample was removed from the bags, placed in jars, and small holes were made in the parafilm. Then the samples were placed in the fridge for approximately 36 hours at 4°C to keep the environmental conditions as close to natural as possible (preincubation). Afterwards, incubation of the soil samples was conducted using the Ultraportable Greenhouse Gas Analyzer (UGGA) LGR ICOSTM GLA132, measuring both CH_4, CO_2 and H_2O. In order to transport the soil samples back to the university, representative sub samples were taken, whereafter the samples were placed in paper bags, wrapped in plastic bags, and brought to Copenhagen.

Laboratory work in Copenhagen

In Copenhagen, pH, carbon and nitrogen analyses were conducted. Soil samples were prepared for pH testing by mixing 10 g of soil with 25 ml of water, and the mixture was shaken for one hour, and tested for pH. For carbon testing, the soil samples were dried in an oven at 103 °C for 22 hours, and then weighted afterwards to obtain soil bulk density. Additionally, soil moisture was calculated as gravimetric soil water content by subtracting the dry weight from the wet weight and dividing the result by the dry weight. Prior to this calculation, the weight of stones and roots were subtracted from both the wet and dry weights. Each sample was then sieved with a 2 mm sieve and prepared for elementary analyses by grinding the soil to dust-sized particles in a mixer mill.

Matlab

The in situ measurements and incubation measurements were separately run through Matlab using a script developed by Eckhardt & Kutzback (2016). In Matlab, raw data from the UGGA, containing continuous data measurements of CH_4, CO_2 and H_2O, and metadata with specific time intervals, volume, area, temperature and thaw depth for each plot, were used as inputs for the script. After the measurements were run through the script, each result was closely examined and adjusted in Matlab. By examining the curves showing the increase in H_2O and CO_2, intervals from the beginning and end of the measurements were cut off if they showed large fluctuations. Since the Matlab script calculates the flux from the slope of the chosen regression model, it was important to choose the model that fitted the data the best. For the in situ measurements enough methane is apparent as substrate in the natural environment, and therefore it is assumed that a linear regression model fits. In contrast, during the incubation, the CH_4 decreases over time in the head space, leading the curve to flatten, making an exponential model better

for these measurements, which is why this model is chosen.

Statistical tests

To test whether the fluxes in the four points differ from each other, the Kruskal-Wallis multiple comparisons test was used. Correspondingly, this was also done with the soil properties. The Kruskal-Wallis test is a nonparametric test that compares three or more groups and concludes if one or more groups differ significantly from the others (McGrew & Monroe, 2014). The test was applied both to determine differences in the three depths between the groups, as well as to test for significant differences between the depths within each group. The tests were carried out in Rstudio and were performed for the flux data as well as for pH, soil moisture, % C, % N and C:N ratio. All tests were carried out with a significance level of $p \leq 0.05$.

All correlation tests were carried out in Excel, using the Regression test function in the Data Analysis package. For all tests including C:N ratio, % C, % N, pH, soil moisture and temperature, the raw value for each sample was used. However, for % dry heath, % fen and plant height, a mean value for each point has been used, because the vegetation replicates were not taken from the exact same locations as the soil samples, and therefore they cannot be paired directly.

Results

Vegetation along the transect

Figure 1 shows the distribution of vegetation in the four points. The green colors indicate that the plant is a part of the vegetation type dry heath, whereas orange colors indicate that the plant is a part of the vegetation type fen. P3 differs from the others by having only the three plants Salix Arctophila, Mos and Grass, which are all a part of the vegetation typer fen. P1, P2 and H are instead all dominated by Cassiope, Betula nana, Salix glauca, Emptrum nigrum and Vaccinium uliginosum, which are all plants belonging to dry heath, although P2 has a small amount of grass of 1.9 %.

Table 1 shows the mean value and the standard deviation for each of the vegetation properties It appears how the plant height decreases from P1 to P3, while H has a similar height as P1. The standard deviations for the plant heights show that the replicates within P1 variates the most followed by the replicates within the hummock. The replicates within P3 have least variation.

Table 1: Table showing plant height, % of dry heath and % of fen ± SE across the transect. Plant height is a mean value of each plant height in all the three replicates for each point.

	Plant height (cm)	% Dry heath	% Fen
P1	9.26 ± 3.86	100 ± 0	0 ± 0
P2	8.83 ± 2.08	98.15 ± 3.2	1.85 ± 3.21
P3	6.00 ± 1.13	0 ± 0	100 ± 0
H	9.55 ± 2.52	100 ± 0	0 ± 0

Fluxes from in situ and laboratory incubations

In Figure 2 the flux data from the laboratory incubations are presented for each depth and replicate along the transect. Likewise, the in situ fluxes are presented in Figure 3. When

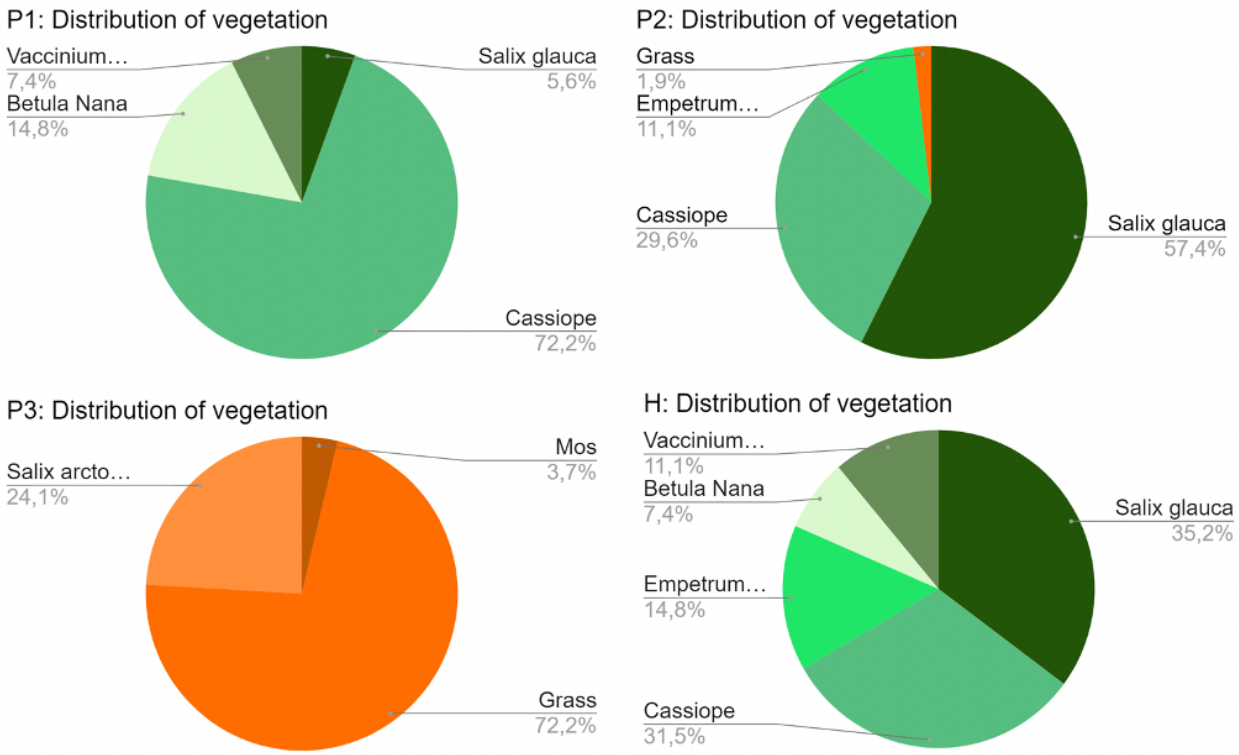

Figur 1: Distribution of vegetation in P1, P2, P3 and H. Distribution of each point is based on the mean of each plant in all three replicates for each point.

looking at the incubation fluxes, a pattern emerges where P1 shows production, P2 shows both cases of consumption and production, P3 predominantly shows production, which is also the highest production along the transect, but also has some spots with consumption. H shows both consumption and production, with production in D1 and consumption in D2 in all replicates. The measurements range between -0.020 g CH_4 s^{-1} m^{-1} and g 0.046 g CH_4 s^{-1} m^{-1}. It is important to emphasize that all the measured incubation fluxes are very small and that they have a very high standard error. This will be discussed further in the discussion. A bar chart with standard errors is presented in Figure A in the appendix.

When looking at the in situ fluxes in Figure 3, some of the same trends can be observed. However these trends are more consistent compared to the incubation fluxes in that the fluxes do not vary between release and uptake within the same point. The in situ fluxes show a relatively high release in P3 and uptake in all other points with the highest uptake in H. The fluxes range between -0,039 g CH_4 s^{-1} m^{-1} and 0,263 g CH_4 s^{-1} m^{-1}. The in situ measurements mostly show higher fluxes compared to the incubation fluxes. The standard errors of the in situ fluxes are not as high as for the incubation fluxes, however, these are also presented in the appendix, Figure B, and discussed further in the discussion.

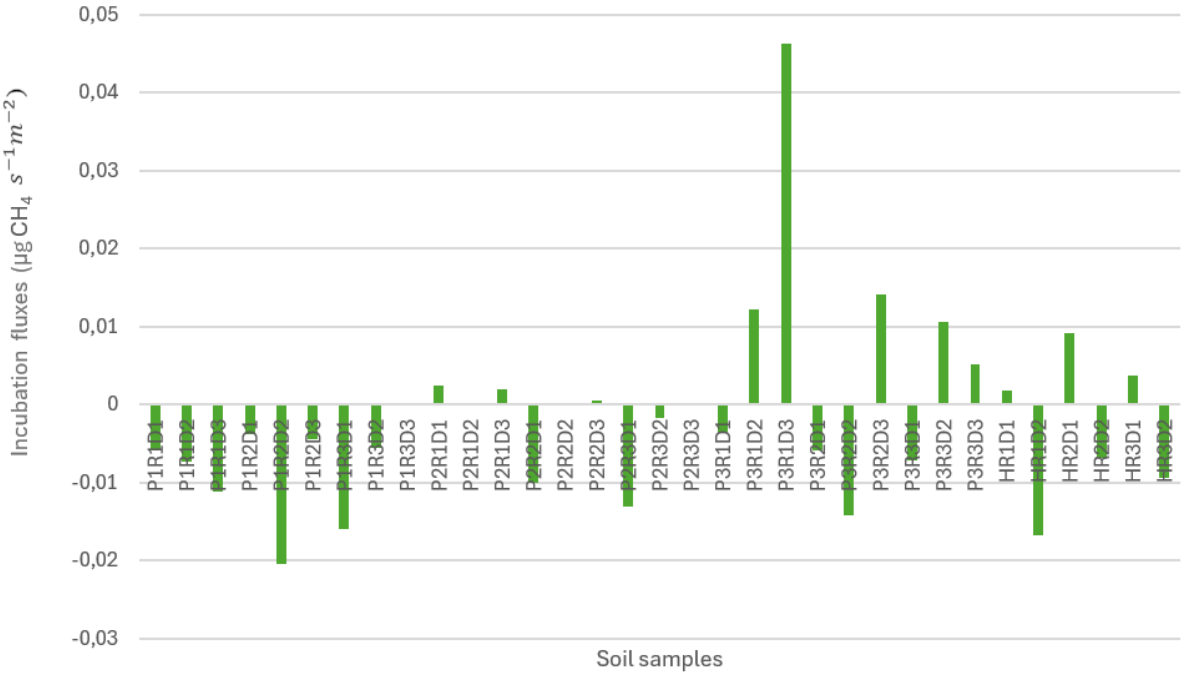

Figure 2: Bar chart showing the measured incubation fluxes in each sample along the transect, sorted in points (P), replicates (R) and depths (D), starting with P1.

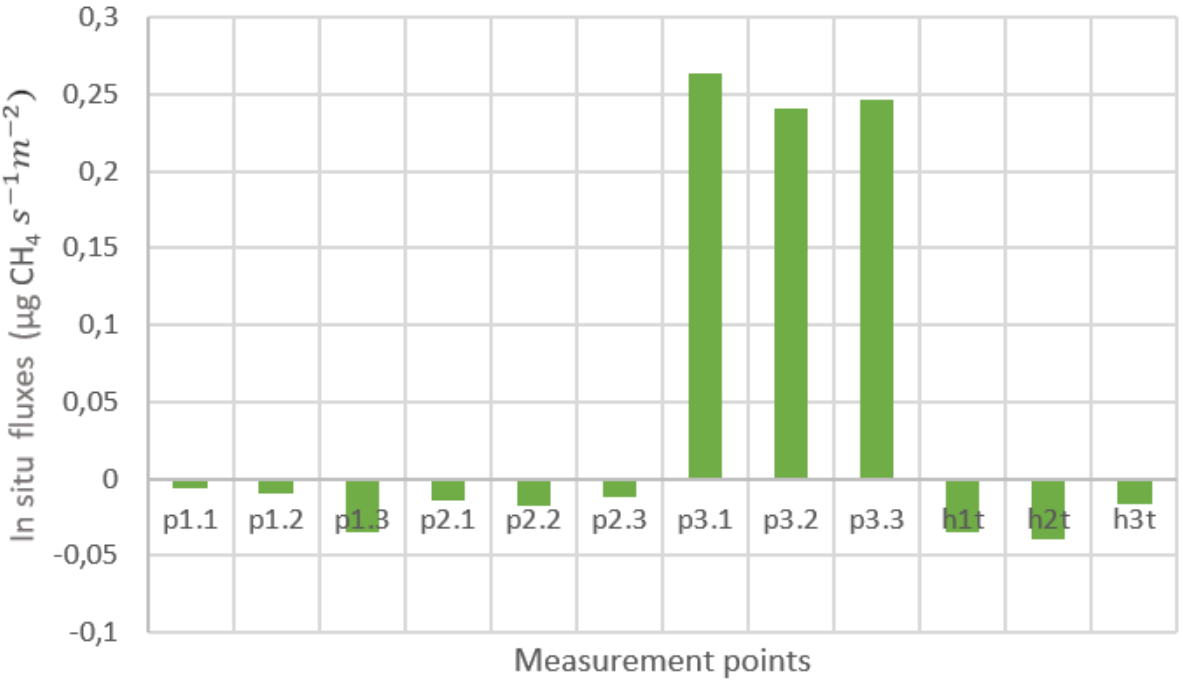

Figure 3: Bar chart showing the measured in situ fluxes in each sample along the transect, sorted in points (P) and replicates (R) starting with P1.

Kruskal-Wallis multiple comparisons tests for incubation fluxes

Figure 4 shows the Kruskal-Wallis multiple comparisons test performed on the incubation fluxes. Mean values ±SE are listed in Table 2. In the following, all described differences between the samples are significant differences ($p \leq 0.05$), unless anything else is specified. The test shows that the CH_4 flux is not different between the groups in D1 and D2, but in D3 they all differ with P3 having the highest production of CH_4, P2 has a slight production and P1 has a small consumption. When looking at the fluxes within the groups, only the depths in H differ, with D1 having a CH_4 production of 0.0049 ± 0.0022 g CH_4 s^{-1} m^{-1} and D2 has a CH_4 consumption of -0.0110 ± 0.0030 g CH_4 s^{-1} m^{-1} .

Kruskal-Wallis multiple comparisons tests for different soil properties

In Table 2, the Kruskal-Wallis multiple comparisons test has been performed on several soil properties, in order to cover significant differences between and within the points. All described differences are significant with $p \leq 0.05$, unless else is specified.

Point 3

Looking at the different test results and mean values, P3 stands out from the other points in several ways. It has a higher % C in D1 compared to P1 and P2, and also a higher % C in D3 compared to the other points, however the latter is not significant since the p-value is 0.06. In terms of pH, P3 has a

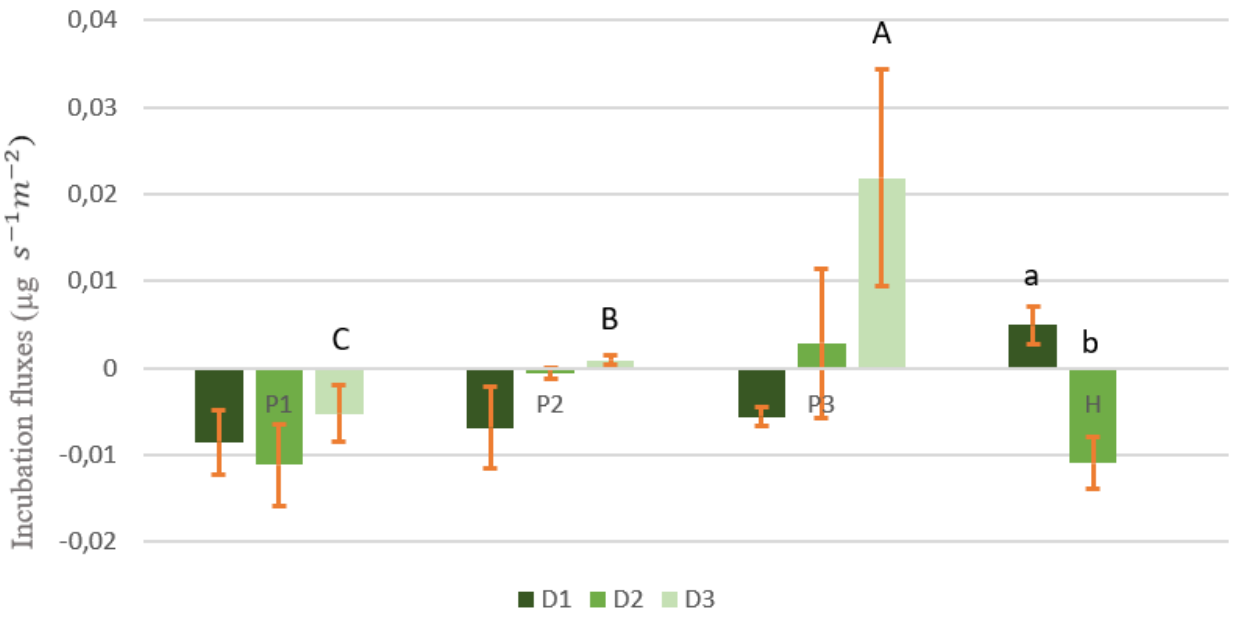

Figure 4: Kruskal-Wallis multiple comparisons test performed on incubation fluxes. Values are averages of the 3 replicates and the orange lines show standard errors (SE) for each depth. Upper case letters indicate significant difference between the points, while lower case letters show significant difference between depths within the same point.

Table 2: Kruskal-Wallis multiple comparisons test performed on incubation fluxes and different soil properties. Values are averages ± SE of the 3 replicates for each depth. Upper case letters indicate significant difference between the points, while lower case letters show significant difference between depths within the same point. All tests are performed on a significant level at $p \leq 0.05$.

	Point 1 D1	Point 1 D2	Point 1 D3	Point 2 D1	Point 2 D2	Point2 D3	Point 3 D1	Point 3 D2	Point 3 D3	H D1	H D2
Flux ($\mu g\ CH_4\ s^{-1}\ m^{-2}$)	-0.0085 ± 0.0037	-0.0111 ± 0.0047	-0.0052 ±0.0032 C	-0.0069 ± 0.0047	-0.0005 ± 0.0006	0.0009 ± 0.0005 B	-0.0056 ± 0.0010	0.0028 ± 0.0085	0.0218±0.0125 A	0.0049±0.002 a	-0.0110±0.0030 b
pH	5.55 ± 0.37 AB b	6.07±0.19 AB ab	6.55 ± 0.036 AB a	5.74 ± 0.36 AB	6.39 ± 0.19 A	6.65 ± 0.09 A	6.58 ± 0.06 A	6.01 ± 0.16 AB	5.99± 0.11 B	4.82 ± 0.06 B b	5.35 ± 0.07 B a
Total C %	21.8 ± 9.66 B	18.3 ± 8.88	2.6 ± 0.27	21.1 ± 2.16 B	8,7 ± 5.26	2.1 ± 0.75	40.2 ± 0.98 A	28.3 ± 3.21	25.9 ± 3.54	40.4 ± 2.08 A	33.9 ± 5.04
Total N %	0.9 ± 0.4	0.8 ± 0.4 B	0.16 ± 0.01	0.99 ± 0.10	0.54 ± 0.29 B	0.15 ± 0.056	1.36 ± 0.24	1.65 ± 0.12 A	1.47 ± 0.03	1.43 ± 0.06	1.74 ± 0.20 A
C:N ratio	22.27 ± 4.75	19.96 ± 2.7	15.75 ± 0.73	21.31 ± 0.95 a	14.63 ± 1.34 b	14.57 ± 0.55 ab	31.44 ± 5.34	17.16 ± 1.52	17.56 ± 2.16	28.4 ± 1.81 a	19.32 ± 0.88 b
Soil moisture (θg)	1.092 ± 0.393 B	1.154 ± 0.451	0.327 ± 0.037	1.283 ± 0.101 B	0.903 ± 0.507	0.298 ± 0.035	8.103 ± 1.129 A	4.909 ± 0.659	4.641 ± 1.378	1.759 ± 0.18 AB	3.238 ± 1.137

higher pH in D1 compared to the other points, but in D3, P3 varies from the other points by having a lower pH. In P3 soil moisture is higher in D1 compared to the other points and in D3, P3 also has a contrasting higher soil moisture compared to the other points, however this is not significant, since the p-value is 0.06.

Hummock

H shares some similar traits with P3, particularly in having a higher % C in D1 compared to P1 and P2. H differs in terms of its C:N ratio, which decreases with increasing depth. In both D1 and D2, H is distinguished by a slightly lower pH compared to the other points, and within H, the pH increases with depth. Furthermore, in D1, H has a different soil moisture compared to the other groups, with higher moisture levels than P1 and P2, but still much lower than P3.

Point 1 and Point 2

P1 and P2 are characterized by lower % C in D1 compared to both P3 and H. Looking at pH in D1, P1 and P2 form a distinct group, being different from both P3 and H, having intermediate pH values. However, in D2 and D3, P2 has a higher pH compared to P3 and H, while P1 has values in a middle range. In P1, the pH values differ across all depths, increasing with depth. Finally, in D1, both P1 and P2 have lower soil moisture levels compared to P3 and H, with considerably lower levels than P3.

Correlations between fluxes and soil properties

Table 4 and Table 5 present the results of correlation tests between both in situ fluxes and laboratory incubation fluxes, and different soil/vegetation properties. Table 4 shows that no significant correlations exist between the incubation fluxes and the soil/vegetation properties. However, the regression between % dry heath and flux has a p-value of 0.09 and af R^2 value of 0.82, and is thus the regression closest to being significant, next followed by the regression between fen and flux, which has a p-value of 0.1 and a R^2 of 0.8. Different results appear when testing the correlations between in situ fluxes and the soil/vegetation properties (Table 5). These regressions all show significant correlations with p-values close to 0. The results show a positive correlation between in situ fluxes and soil moisture, and a negative correlation between in situ fluxes and temperature. When it comes to vegetation, the tests show negative correlations with plant height and % dry heath, but a positive correlation with % fen.

Table 4: Correlations between incubation fluxes and different soil- and vegetation properties.

Correlation test between incubation fluxes and different parameters			
	R^2	P-value	Linear regression formula
C:N ratio	0,010	0,56	y = -55,907x + 20,122
Total % N	0,04	0,24	y = 10,799x + 1,0347
Total % C	0,009	0,59	y = 118,31x + 22,313
pH-value	0,0004	0,91	y = -1,0598x + 5,9706
Soil moisture θg	0,01	0,54	y = 23,563x + 2,5581
Plant height (cm)	0,66	0,18	y = -46,954x + 7,461
% Dry heath	0,82	0,09	y = -7356,1x + 60,356
% Fen	0,8	0,1	y = 7370,8x + 38,633

Table 5: Correlations between in situ fluxes and different soil- and vegetation properties. Soil moisture and temperature are measured in 10 cm depth.

Correlation test between in situ fluxes and different parameters			
	R^2	P-value	Linear regression formula
Soil moisture θg	0,600	0,002	y = 121,5x + 25,294
Temperature °C	0,52	0,007	y = -5,009x + 6,2856
Plant height (cm)	0,98	0,007	y = -46,954x + 7,461
% Dry heath	0,99	0,0011	y = -361,95x + 90,524
% Fen	0,99	0,0009	y = 366,59x + 8,22

Discussion

Fluxes

Overall, our flux results from both in situ and from incubation align with what we expected based on the theory. We predominantly observe uptake at points located in dry heath and release at the point located in the fen. However, the incubation of hummock does not correspond with theory, as a production in D1 and a consumption in D2 is seen. This might be because of rain in the topsoil, which was retained from infiltration by the vascular plant tissue. In addition, consumption in D2 might be due to oxygen transportation through the sides of the hummock. Furthermore, the plant height decreases downhill, which might be explained by a longer growing season uphill. The hummock has the highest plant height, which might be due to snow and water accumulation in the hollow parts, leaving the top free of snow for plant growth.

In terms of measurement reliability, it is normally expected that the measurements taken in the laboratory would be more controlled, because it is possible to create a closed system, whereas the in situ measurements represent a snapshot of the natural conditions, which may vary over a short time. Nevertheless, the opposite applies here, where lower error bars are seen for the in situ fluxes compared to the incubation fluxes. However, the in situ measurements cover a larger area and provide significantly more data than the laboratory results, which could result in lower error bars. The in situ fluxes show significant correlations with all soil properties, whereas the incubation fluxes show no significant correlation with any of the measured properties. The laboratory results may have been influenced by various factors during the experimental process. The samples were repeatedly taken in and out of refrigeration, and they were handled outside of their storage bags, potentially causing compression. Some of the laboratory work was conducted on Disko, while other parts were completed in Copenhagen. During transport, the samples were carried by students and exposed to varying air temperatures and humidity levels while still in plastic bags.

Soil moisture and temperature

Soil moisture is, as described in the theory section, one of the most significant soil properties controlling methane fluxes. However, the laboratory results show no correlation with this property. In the topsoil of P3, a soil moisture of 8.103 ± 1.129 θg was measured, which is significantly higher than in the other points. D'Imperio et al. (2016) have also examined the fluxes and soil properties in different parts of Blæsedalen and find a significantly higher soil moisture in the fen compared to in the dry heath. Nevertheless, they find that the fen have 2.88 times higher soil moisture than dry heath, whereas a ratio of 6.82 is found in this study. However, the calculated soil moisture is associated with many different uncertainties and errors. The soil moisture was calculated by weighing the soil samples before and after drying, and subtracting the weight of rocks and stones from both the wet weight and dry weight, after being transported back to Copenhagen. Ideally, the samples should have been wet-sieved from the start to remove rocks and stones

immediately, and the soil moisture should have been measured after incubation. Furthermore, the soil samples were not kept in their natural environment but exposed to temperature changes and handled on paper, before the soil moisture was measured, which may have decreased the soil water content. In contrast, the in situ fluxes show a strong positive correlation with soil moisture, which is also expected in this area (D'Imperio et al., 2016). In the field, the in situ soil moisture was measured directly 10 cm down in the soil, which means that the soil has not been exposed to the same errors, as described above, making them more trustworthy.

The significant correlation between in situ fluxes and temperature shows that the lower the temperature, the higher the flux. Similar trend is seen in D'Imperio et al. (2016), showing a higher temperature in dry heath and a lower in fen. The correlation between in situ fluxes and temperature can maybe be explained by the fact that in Blæsedalen, the CH_4 flux reaction increases significantly with increase in soil temperature in dry heath, whereas no correlation is seen in fen, according to D'Imperio et al., (2016). This might be a sign that the CH_4 consuming microorganisms are more sensitive to temperature changes, og thus maybe consumes less CH_4 in P3 than uphill, affecting the amount of net production. This theory aligns with what Nielsen et al., (2017) concludes in their study, in that they find that high-affinity methanotrophs have a higher temperature sensitivity compared to the temperature sensitivity of methanogenesis.

C:N ratio and % C

The C:N ratio was higher for the fen than the dry heath. However, grass typically has a low C:N ratio, thus opposite trend was observed. The vegetation is too uniform to show a significant difference in C:N ratio, however if grass had been more dominant in the dry heath areas, a significant difference corresponding with theory might have been measured. However, the hummock, which is also covered by dry heath vegetation, has the highest measured C:N ratio, which align with expectations.

With regards to carbon content, a higher carbon content was measured for fen and hummock compared to the two dry heath areas, however only significantly in the topsoil. The carbon content of the topsoil in P3 D1 was measured to 40.2 ± 0.98 % C, which is considerably high compared to D'Imperio et al. (2016), where a % C of 21.08 ± 1.50 was seen in the topsoil of the fen. Similarly the hummock was measured to 40,4 ± 2.08. This might be due to the fact that considerably more roots were entangled in these soil samples, which was impossible to remove without wet-sieving. Therefore, roots have been included in carbon testing for the fen and hummock, but not for two dry heath areas, leading to a higher carbon content.

Soil pH

In the fen, pH values of 6.58 ± 0.06 and 6.01 ± 0.16 were measured, which are slightly more acidic than those reported for fens by D'Imperio et al. (2016), who measured pH values of 7.15 ± 0.07 and 6.88 ± 0.09 at 0-5 cm and 5 cm depths, respectively. However,

the pH is significantly lower in P1 and P2, consistent with findings from D'Imperio et al. (2016), who similarly reported a pH of 5.08 ± 0.09 in the topsoil of dry heath. In general, H has a lower pH than the others. The pH doesn't vary much across the transect and the soil is relatively acidic, which dissolves carbonates. Therefore, it can be assumed that the carbon in the soil is organic.

Comparison with CH_4-budget from D'Imperio et al. (2016)

D'Imperio et al. (2016) calculates the total CH_4 budget of Blæsedalen based on in situ measurement all taken during three months (90 days) in the growing season. The in situ fluxes from this report can be scaled up and compared to the findings in D'Imperio et al. (2016) since the same vegetation types are identified. D'Imperio et al. (2016) divides the area of Blæsedalen into three different vegetation covers; dry heath, bare soil and fen, whereas in this report only finds dry heath and fen. D'Imperio et al. (2016) finds that dry heath constitutes 103,253 m^2, whereas fen constitutes 23,467 m^2 in Blæsedalen. D'Imperio et al. (2016) finds that dry heath has a seasonal integrated flux of -0.10 ± 0.02 g CH_4 -C m^2 and the fen area has a seasonal flux of 0.10 ± 0.01 g CH_4 -C m^2. When scaling up the in situ fluxes in this project from seconds to 90 days and the microgram to gram the dry heath areas has a seasonal flux of -0.12 g CH_4 -C m^2, which is quite close to the findings in D'Imperio et al. (2016). The fen areas, however, have a seasonal flux of 1.46 g CH_4 -C m^2, which is considerably higher than D'Imperio et al. (2016) finds.

D'Imperio et al. (2016) also calculates the total CH_4 budget by including the different areas of each vegetation type, and finds that Blæsedalen has a net uptake of -12.71 kg CH_4-C. Making the same calculations for this project, Blæsedalen also has a net uptake, but only of -3.77 kg CH_4-C. Of course, the measurements in this report are not representative for the whole growing season, since the measurement is only carried out on one single day in August, and is thus not covering differences within the season. In addition to this, D'Imperio et al. (2016) results are based on significantly more samples than our results. Furthermore, a lot of precipitation had fallen prior to the fieldwork, which may have increased the methane production. However, this rough estimate indicates that Blæsedalen is a net sink of CH_4, even during a wet summer.

Conclusion

The laboratory incubations showed a net consumption of CH_4 in P1 and P2, highest in P1, a net production in P3 and a net consumption in the H. P1 only had consumption, while P2 had a small production in D3. P3 only consumed CH_4 in D1 and had a high production of CH_4 in D3, whereas H produced CH_4 in D1, but consumed in D3. However, H had CH_4 production in D1, which wasn't expected, which might be due to precipitation before measurements. Similarly, the in situ measurements show an uptake in P1, P2 and H, with highest uptake in H, and release in P3. The in situ fluxes correlated strongly with dry heath, fen and plant height, showing that the higher % of dry heath the lower the flux, the higher % fen the higher the flux, and the

higher the plant height the lower the flux. Furthermore, with both soil moisture and temperature the correlations show that higher soil moisture results in a higher flux and lower temperatures result in a higher flux. On the other hand, the soil properties do not correlate with the incubation fluxes. However, if a significant level of 0.1 had been used, dry heath and fen would have correlated with the fluxes, implying that there is a trend between these vegetation types, and respectively uptake and release of CH_4. When it comes to the differences between the soil properties between and within each point and depth, several conclusions can be drawn. With regard to soil moisture, P3 has significantly more soil moisture in D1, H has significantly more than P1 and P2, with these being similar. The same pattern is expressed in % C, whereas P3 and H have significantly higher C % than P1 and P3, which must be due to more plant roots in the soil. However, the % C in these may also have been overestimated due to inclusion of root material in carbon testing. On the other hand, C:N ratios did not correspond with what was expected, as the highest ratio was seen in P3, and lowest in P1 and P2. The opposite would have been expected, since plant distribution controls the C:N ratio. With regards to pH, the soil is relatively acidic and ranges between 4.82±0.06 and 6.65± 0.09. Trying to scale up the measured CH_4 fluxes to the entire Blæsedalen in the growing season, it is concluded that Blæsedalen is a net sink with an uptake of -3,77 kg CH_4-C. Even though this calculation is based on a rough estimate, it gives an indication of the overall CH_4-environment in Blæsedalen.

References

Christiansen, J. R., D'Imperio, L. & Elberling, B. (2024). Mikroorganismer i jorden vender op og ned på methanregnskabet. *Aktuel naturvidenskab* nr. 1 (2024), s. 36-40.

Christiansen, J. R., Romeo, A. J. B., Jørgensen, N. O. G., Glaring, M. A., Jørgensen, C. J., Berg, L. K. & Elberling, B. (2014). Methane fluxes and the functional groups of methanotrophs and methanogens in a young Arctic landscape on Disko Island, West Greenland. *Biogeochemistry*, (2015) 122:15–33. DOI: 10.1007/s10533-014-0026-7

D'Imperio, L., Nielsen, C. S., Westergaard-Nielsen, A., Michelsen, A. & Elberling, B. (2016). Methane oxidation in contrasting soil types: responses to experimental warming with implication for landscape integrated CH4 budget. *Global Change Biology* (2017) 23, 966–976. DOI: 10.1111/gcb.13400

D'Imperio, L., Bing-Bing, L., Tiedje, J. M., Oh, Y., Christiansen, J. R., Kepfer-Rojas, S., Westerdaard-Nielsen, A., Brandt, K. K., Holm, P. E.,Wang, P., Ambus, P. & Elberling, B. (2023). Spatial controls of methane uptake in upland soil across climatic and geological regions in Greenland. *Communications Earth & Environment* (2023)4:461. DOI: 10.1038/s43247-023-01143-3

Eckhardt, T. & Kutzbach, L. (2016): Matlab code to calculate gas fluxes from chamber-based methods [dataset]. *Institut für Bondekunde, Universität Hamburg, Pangea*. DOI: 10.1594/PANGAEA.857799

Elberling, B. (2020). Biogeichemical cycles & impacts in society. *University of Copenhagen, Department of Geosciences and natural resource management*

McGrew, J.C. and Monroe, C. (2014). An Introduction to Statistical Problem Solving in Geography. 3rd edition, *McGraw Hill*, ISBN: 0-697-22971-8

Nielsen, C. S., Michelsen, A., Strobel, B. W., Wulff, K., Banyasz, I. & Elberling, B. (2017). Correlations between substrate availability, dissolved CH4, and CH4 emissions in an arctic wetland subject to warming and plant removal. J. Geophys. Res. Biogeosci. 122, 645–660. DOI:10.1002/2016JG003511.

Ruiz-Fernández, J., Oliva, M., Otero, X. L., & García-Hernández, C. (2020). Morphometric and sedimentological characteristics of Late Holocene earth hummocks in the Zackenberg Valley (NE Greenland). *Science of the Total Environment*, *737*, 140281. DOI: 10.1016/j.scitotenv.2020.140281

Sullivan, P. F., Arens, S. J. T., Chimner, R. A. & Welker, J. M. (2007). Temperature and Microtopography Interact to Control Carbon Cycling in High Arctic Fen. *Ecosystems* (2008) 11:61-76. DOI: 10.1007/s10021-007-9107-y

Appendix

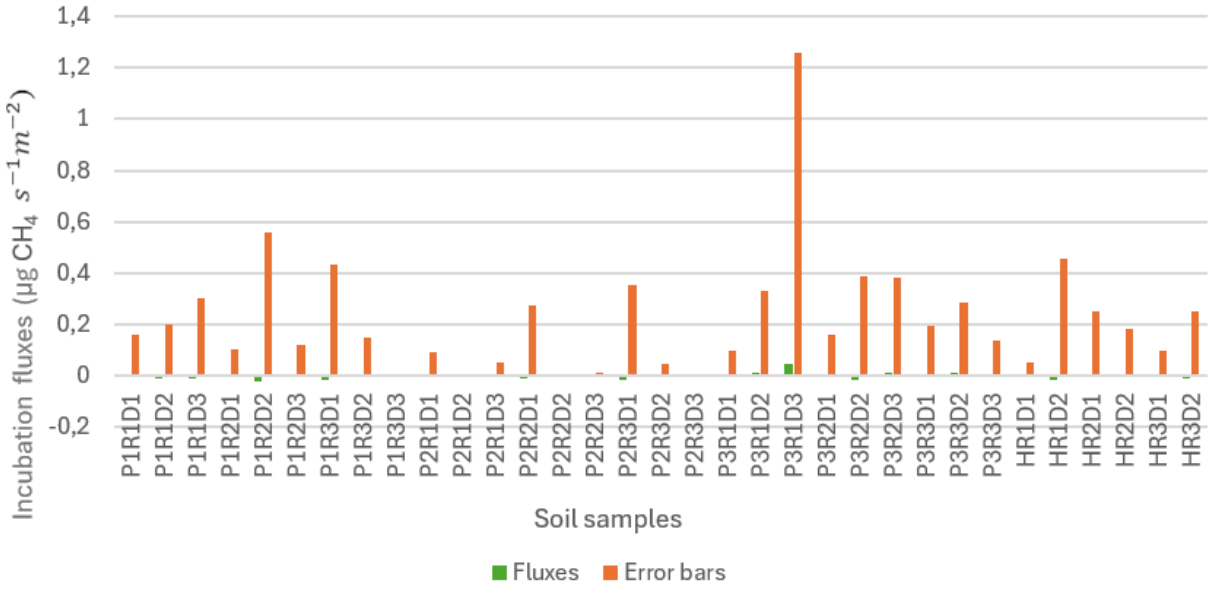

Figure A: Bar chart showing incubation fluxes and error bars.

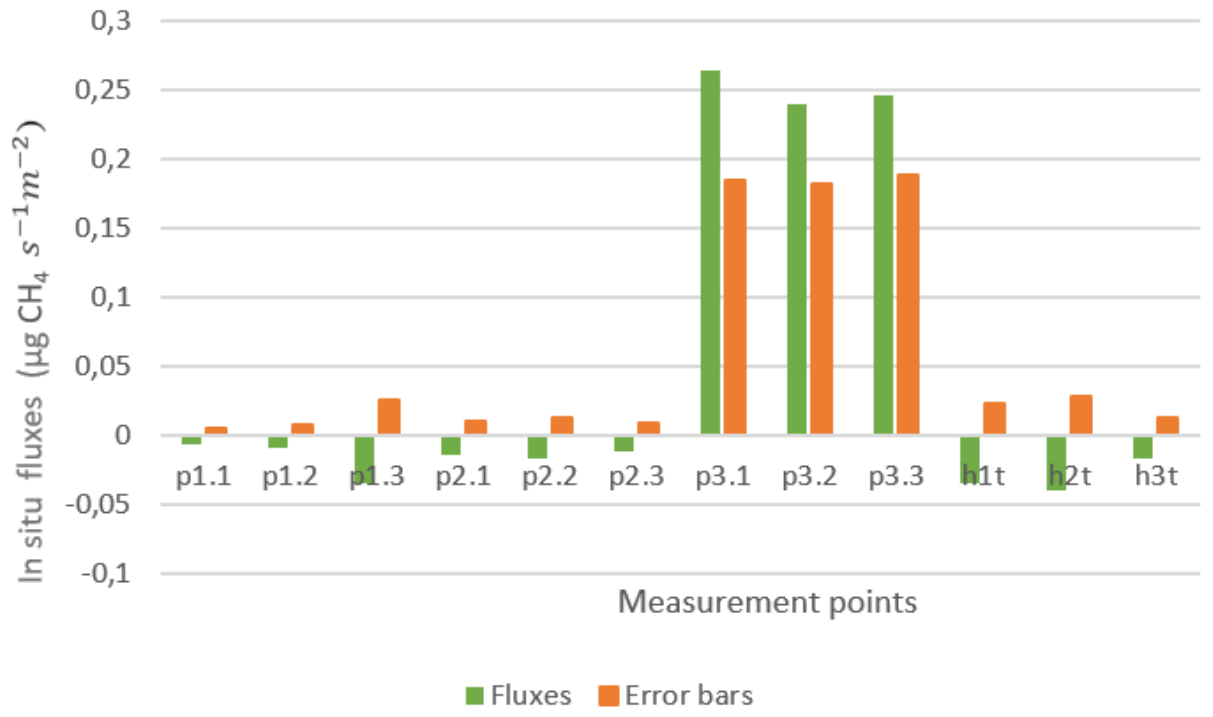

Figure B: Bar chart showing in situ fluxes and error bars.